J. Fluid Mech. (2004), *vol.* 504, *pp.* 183–211.
DOI: 10.1017/S0022112004008006 Printed in the United Kingdom

Numerical study of the instability of the Hartmann layer

By D. S. KRASNOV[1], E. ZIENICKE[1], O. ZIKANOV[2], T. BOECK[3] AND A. THESS[1]

[1]Fakultät für Maschinenbau, Technische Universität Ilmenau, PF 100565, 98684 Ilmenau, Germany
thess@tu-ilmenau.de

[2]Department of Mechanical Engineering, University of Michigan – Dearborn, Dearborn, MI 48128-1491, USA

[3]Laboratoire de Modélisation en Mécanique, Université Pierre et Marie Curie, 8 rue du Capitaine Scott, 75015 Paris, France

(Received 7 March 2003 and in revised form 1 July 2003)

Direct numerical simulation is applied to investigate instability and transition to turbulence in the flow of an electrically conducting incompressible fluid between two parallel unbounded insulating walls affected by a wall-normal magnetic field (the Hartmann flow). The linear stability analysis of this flow provided unrealistically high critical Reynolds numbers, about two orders of magnitude higher than those observed in experiments. We propose an explanation based on the streak growth and breakdown mechanism described earlier for other shear flows. The mechanism is investigated using a two-step procedure that includes transient growth of two-dimensional optimal perturbations and the subsequent three-dimensional instability of the modulated streaky flow. In agreement with recent experimental investigations the calculations produce a critical range between 350 and 400 for the Hartmann thickness based Reynolds number, where the transition occurs at realistic amplitudes of two- and three-dimensional perturbations.

1. Introduction

Several well-known systems in fluid dynamics show a transition to turbulence that is not triggered by the linear instability of a basic state – as for example in Rayleigh–Bénard or the Taylor–Couette systems – but appears long before the critical parameter for the linear instability is reached. Typical examples are plane Poiseulle flow with a critical Reynolds number based on linear theory $Re_c \approx 5772$ and pipe flow, which never becomes unstable to infinitesimal perturbations. For plane Poiseulle flow, transition to turbulence occurs around $Re \approx 1000$ and for pipe flow at $Re \approx 2000$. This kind of transition is typical for shear flows and characterized by the following features:

(*a*) the transition to turbulence has no sharp 'critical' Reynolds number;

(*b*) initial perturbations of finite strength are necessary to excite the transition;

(*c*) after the transition, many degrees of freedom over a large range of length and time scales are immediately present in the turbulence.

In the past decade, considerable advances have been made towards a better theoretical understanding of this kind of transition (see Grossmann 2000 or Schmid & Henningson 2001 for a review). It has been shown that a strong transient growth of certain perturbations is possible because of the non-normality of the linear operator

of the flow (see Schmid & Henningson 2001 and references therein). In the linearized formulation, the perturbations would eventually decay after the transient growth because all eigenvalues of the system correspond to linearly stable modes. But, if the transient growth is large enough, the nonlinearity has to be taken into consideration. It can be shown that the modulated flow is unstable to three-dimensional perturbations with their amplitude being dependent, in general, on flow parameters. Thus, a two-step mechanism was proposed to explain the features of transition to turbulence in shear flows consisting of (i) a large transient growth of small (but not infinitely small) two-dimensional disturbances leading to a modulation of the basic flow, and (ii) the linear instability of the modulated flow with respect to three-dimensional perturbations.

The purpose of the present paper is to apply this concept to a flow of an electrically conducting incompressible fluid between two parallel unbounded insulating walls in the presence of a uniform magnetic field $\boldsymbol{B}_0$ acting in the wall-normal direction (Hartmann & Lazarus 1937, figure 1). The motivation of our work is twofold. First, our system, which we shall refer to as magnetohydrodynamic (MHD)-channel flow or Hartmann flow, represents an example where the discrepancy between the prediction of the linear stability analysis and experimental observation is practically challenging. Second, recent experiments (Moresco & Alboussière 2004), performed with unprecedented accuracy and coverage of the parameter space, have created a comprehensive set of reliable transition data, which call for a thorough theoretical analysis.

The shape of the basic velocity profile is determined by the value of the non-dimensional Hartmann number

$$Ha = B_0 L \sqrt{\frac{\sigma}{\rho \nu}}, \tag{1}$$

where σ is the electric conductivity of the liquid, ρ and ν are its density and kinematic viscosity, and L is the channel width. If the Hartmann number is large, the velocity profile consists of a flat part corresponding to the bulk flow and two Hartmann boundary layers at the walls, in which the whole shear stress is concentrated and where the induced electric currents are closed (see e.g. Davidson 2001). The Hartmann layers have the thickness $\delta = L/Ha$. For sufficiently large Hartmann number, the two Hartmann layers do not overlap and can be considered as independent from each other. We note that $Ha \to 0$ corresponds to the non-magnetic case with a parabolic velocity profile.

The appropriate parameter to describe the stability of a single Hartmann layer is the Reynolds number R, based on the Hartmann layer thickness:

$$R = \frac{U\delta}{\nu} = \frac{UL}{\nu}\frac{1}{Ha} = \frac{Re}{Ha},$$

where $Re = UL/\nu$ represents the Reynolds number based on the channel width L and the centreline velocity U. This was first observed by Lundquist (1952). Early results for the linear instability were obtained by Lock (1955), who found $R_c \approx 50\,000$, neglecting Lorentz forces acting on the disturbances, and by Roberts (1967), who corrected the limit to $R_c \approx 46\,200$. More recently, a stability analysis using numerical techniques for modified plane Poiseulle flow and modified plane Couette flow in the presence of a transverse magnetic field (Takashima 1996, 1998) produced a critical Reynolds number of $R_c = 48\,311.016$ for sufficiently high Hartmann number. An isolated Hartmann layer was investigated numerically by Lingwood & Alboussiére (1999) who studied the cases of electrically insulating and conducting walls with normal and arbitrarily oriented magnetic field. For the flow considered here, i.e. for

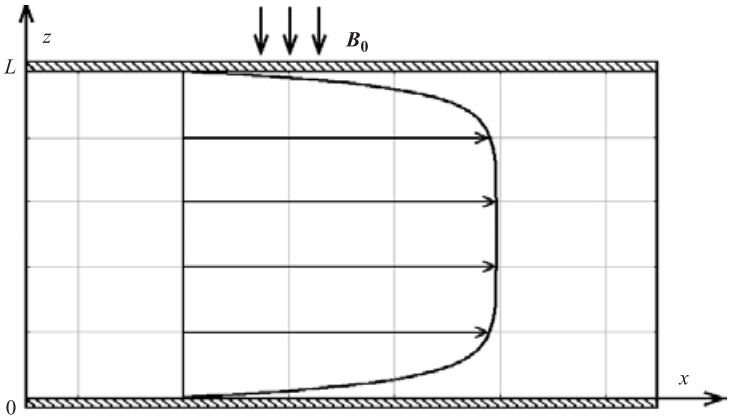

FIGURE 1. Sketch of the flow geometry considered, with a Hartmann profile between two insulating parallel planes. The magnetic field is assumed to be homogeneous and time independent.

the case of insulating walls and vertical magnetic field, they found $R_c = 48\,250$, which differs only slightly from the results of Takashima.

Most experiments exploring the transition regime between laminar and turbulent flow were carried out as laminarization experiments. They did not show the transition from the laminar to the turbulent regime, but, instead, were meant to determine at which values of $R = Re/Ha$ a turbulent flow becomes laminar if it passes through a transverse magnetic field. The results of these experiments showed the re-laminarization to take place in the range $150 \leqslant R \leqslant 250$ (depending on the aspect ratio of the ducts, see Hartmann & Lazarus 1937, Murgatroyd 1953, Lykoudis 1960 and Branover 1967). Recently, Moresco & Alboussiére (2004) carried out an experiment starting from a laminar flow and investigated the transition to turbulence, which was identified by measuring the friction factor for increasing values of R. For a smooth-wall transition, a critical value of $R_c \approx 380$ was found. For the inverse process of re-laminarization, the same critical value of R_c was found without a visible hysteresis.

The situation described above is clearly reminiscent of the transition to turbulence observed with other shear flows. The actual transition takes place at a Reynolds number Re/Ha that is orders of magnitude smaller than the value found for linear instability by the classical stability analysis. We start our investigation with the hypothesis that the transition occurs according to the two-step scenario outlined above. The rest of the paper is devoted to numerical verification of this assumption.

The paper organized as follows. In § 2 we formulate the problem and describe the numerical method used for its solution. The results of numerical experiments are presented in § 3. Concluding remarks are given in § 4. The results of an additional study on streak formation are given in the Appendix.

2. Numerical model

2.1. *Physical formulation and governing equations*

We consider the MHD channel flow shown in figure 1 and assume that the hydrodynamic Reynolds number is large whereas the magnetic Reynolds number is small:

$$Re = \frac{UL}{\nu} \gg 1, \quad Re_m = \frac{UL}{\eta} \ll 1. \tag{2}$$

Here $\eta = (\sigma\mu)^{-1}$ is the magnetic diffusivity, μ is magnetic permeability of free space and σ is the electric conductivity of the fluid.

The assumption of small Re_m is important because it separates the magneto-hydrodynamics of liquid metals from the 'classical' counterpart dealing with astrophysical, geophysical, or plasma flows characterized by large values of Re_m. It can be shown (see, for example, Davidson 2001) that if Re_m and the magnetic Prandtl number $P_m = Re_m/Re$ are small, the so-called quasi-steady approximation can be applied. The fluctuations $\boldsymbol{b}$ of the magnetic field due to fluid motions are much smaller than the applied magnetic field $\boldsymbol{b} \ll \boldsymbol{B}_0$. Furthermore, $\boldsymbol{b}$ and the electric current perturbations $\boldsymbol{j}$, induced by the movement of the electrically conducting fluid across the magnetic field lines, adjust instantaneously to the time-dependent velocity field. The Lorentz force, defined per unit of volume, takes the form

$$\boldsymbol{F} = \boldsymbol{j} \times (\boldsymbol{B}_0 + \boldsymbol{b}) \approx \boldsymbol{j} \times \boldsymbol{B}_0, \tag{3}$$

where $\boldsymbol{j}$ is defined according to Ohm's law

$$\boldsymbol{j} = \sigma[-\nabla\phi + \boldsymbol{v} \times (\boldsymbol{B}_0 + \boldsymbol{b})] \approx \sigma[-\nabla\phi + \boldsymbol{v} \times \boldsymbol{B}_0], \tag{4}$$

The solenoidal character of $\boldsymbol{j}$ provides the Poisson equation for the electrostatic potential ϕ:

$$\nabla^2\phi = \boldsymbol{B}_0 \cdot \boldsymbol{\omega} = B_0\omega_z, \tag{5}$$

where $\boldsymbol{\omega}$ is the flow vorticity.

The accuracy of the quasi-steady approximation (3)–(5) has been confirmed in numerous investigations of various low-Re_m flows (see e.g. Davidson 2001 and references therein). For the particular case of a turbulent channel flow in a transverse magnetic field, Lee & Choi (2001) verified the validity of the approximation through a comparison of solutions of (6) with solutions of the full MHD equations.

For the non-dimensional formulation of the problem we use the centreline velocity U_0, channel width L and applied magnetic field B_0 as the typical scales for velocity, length and magnetic field, respectively. Further, we derive the time scale L/U_0, pressure scale ρU_0^2, and the scales for electric current and potential $\sigma B_0 U_0$ and $L B_0 U_0$, respectively. The non-dimensional governing equations and boundary conditions are then

$$\left.\begin{aligned} &\frac{\partial \boldsymbol{v}}{\partial t} + (\boldsymbol{v}\cdot\nabla)\boldsymbol{v} = -\nabla p + \frac{1}{Ha\,R}\nabla^2\boldsymbol{v} + \frac{Ha}{R}(\boldsymbol{j} \times \boldsymbol{e}_z), \\ &\boldsymbol{j} = -\nabla\phi + \boldsymbol{v} \times \boldsymbol{e}_z, \\ &\nabla^2\phi = \omega_z, \\ &\nabla\cdot\boldsymbol{v} = 0, \\ &v = 0, \quad \frac{\partial\phi}{\partial z} = 0 \quad \text{at} \quad z = 0, 1. \end{aligned}\right\} \tag{6}$$

To finish this discussion it is necessary to remark that we assume the flow to be driven by a specified volume flux, rather than a given value of the pressure gradient. In the same way the total current is prescribed and is set to zero in spanwise direction $\int_0^1 \boldsymbol{j}_y \, \mathrm{d}z = 0$ and, therefore, the gradient of electric potential

$$\frac{\partial\phi}{\partial y} = -\int_0^1 v_x \, \mathrm{d}z.$$

2.2. *Numerical method*

The three-dimensional flow solver used in this study was initially designed, tested and extensively used for direct numerical simulations of surface-tension-driven (Marangoni) convection (Boeck & Thess 1999). Due to the similarity of mathematical formulation, it can be easily modified for the case of an incompressible fluid flow affected by a homogeneous magnetic field. The flow is computed in a three-dimensional rectangular domain with periodic boundary conditions in both horizontal directions and the no-slip condition at the walls.

The system (6) is solved using a pseudo-spectral numerical method based on Fourier series in the horizontal directions and a Chebyshev polynomial expansion in the vertical direction (Canuto *et al.* 1988; Gottlieb & Orzag 1977). Because of the incompressibility only two velocity components are independent. The velocity field can be represented in terms of two scalar quantities Ψ and Φ using the poloidal–toroidal decomposition (Thual 1992)

$$\boldsymbol{v}(x, y, z, t) = \nabla \times (\nabla \times \boldsymbol{e}_z \Phi(x, y, z, t)) + \nabla \times \boldsymbol{e}_z \Psi(x, y, z, t). \tag{7}$$

Equations for Ψ and Φ are derived by taking the curl and twice the curl of the momentum equation and projecting onto the vertical direction. This results in two equations for the vertical velocity component $v_z = -\Delta_h \Phi$ and the vertical vorticity component $\omega_z = -\Delta_h \Psi$, where $\Delta_h = \partial_x^2 + \partial_y^2$ denotes the horizontal Laplace operator. The quantities v_z and ω_z determine the velocity field up to a mean flow $U(z)\boldsymbol{e}_x + V(z)\boldsymbol{e}_y$. Equations for U and V are obtained by averaging the momentum equation over horizontal cross-sections of the periodicity domain. Upon introducing the definitions

$$\zeta = \omega_z, \quad \eta = \nabla^2 v_z, \quad \xi = v_z \tag{8}$$

for ease of notation, the evolution equations based on the poloidal–toroidal representation take the form

$$\nabla^2 \zeta - R\,Ha \frac{\partial \zeta}{\partial t} - Ha^2 \frac{\partial^2 \phi}{\partial z^2} = F, \tag{9}$$

$$\nabla^2 \phi = \zeta, \tag{10}$$

$$\nabla^2 \eta - R\,Ha \frac{\partial \eta}{\partial t} + Ha^2 \frac{\partial^2 \xi}{\partial z^2} = G, \tag{11}$$

$$\nabla^2 \xi = \eta, \tag{12}$$

$$\frac{\partial^2 U}{\partial z^2} - R\,Ha \frac{\partial U}{\partial t} - Ha^2 U = R\,Ha \left[\frac{\partial \langle v_x v_z \rangle}{\partial z} + \left\langle \frac{\partial p}{\partial x} \right\rangle + \frac{Ha}{R} \left\langle \frac{\partial \phi}{\partial y} \right\rangle \right], \tag{13}$$

$$\frac{\partial^2 V}{\partial z^2} - R\,Ha \frac{\partial V}{\partial t} - Ha^2 V = R\,Ha \left[\frac{\partial \langle v_y v_z \rangle}{\partial z} + \left\langle \frac{\partial p}{\partial y} \right\rangle - \frac{Ha}{R} \left\langle \frac{\partial \phi}{\partial x} \right\rangle \right]. \tag{14}$$

The angular brackets $\langle\rangle$ denote horizontal averages, and the symbols F and G stand for the nonlinear terms:

$$F = -R\,Ha\, \boldsymbol{e}_z \cdot \nabla \times (\boldsymbol{v} \times \boldsymbol{\omega}), \tag{15}$$

$$G = R\,Ha \left[\frac{\partial \nabla \cdot (\boldsymbol{v} \times \boldsymbol{\omega})}{\partial z} - \boldsymbol{e}_z \cdot \nabla^2 (\boldsymbol{v} \times \boldsymbol{\omega}) \right]. \tag{16}$$

We note that each of the evolution equations is of second order, i.e. one boundary condition is needed at the top and the bottom for $\zeta, \phi, \eta, \xi, U$ and V. The appropriate boundary conditions are readily derived using the incompressibility

constraint $\nabla \cdot \boldsymbol{v} = 0$. We obtain

$$\xi = \zeta = \frac{\partial \phi}{\partial z} = \frac{\partial \xi}{\partial z} = U = V = 0. \tag{17}$$

The condition $\partial \xi / \partial z = 0$ represents the boundary condition for the η-equation.

In order to derive a discrete representation of (9)–(12) we introduce ζ_k, η_k, ξ_k and ϕ_k as the Fourier coefficients of the mode with wave vector $\boldsymbol{k} = k_x \boldsymbol{e}_x + k_y \boldsymbol{e}_y$. For time differencing we use the implicit backward Euler scheme for the linear terms and the explicit second-order Adams–Bashforth scheme for nonlinear terms. The absolutely stable backward Euler scheme, in spite of being only first-order accurate, was chosen to avoid problems of numerical instability for the highest wavenumbers. Advancing the solution from the time level n to $n+1$ requires the solution of four linear second-order boundary value problems for each wave vector. They are

$$\left(\mathrm{D}^2 - \boldsymbol{k}^2 - \frac{R\,Ha}{\Delta t} - Ha^2 \right) \zeta_k^{n+1} - \boldsymbol{k}^2 Ha^2 \phi_k^{n+1} = -\frac{R\,Ha}{\Delta t} \zeta_k^n + AB\,\{F_k\}^n, \tag{18}$$

$$(\mathrm{D}^2 - \boldsymbol{k}^2)\phi_k^{n+1} - \zeta_k^{n+1} = 0, \tag{19}$$

$$\left(\mathrm{D}^2 - \boldsymbol{k}^2 - \frac{R\,Ha}{\Delta t} \right) \eta_k^{n+1} + Ha^2 \mathrm{D}^2 \xi_k^{n+1} = -\frac{R\,Ha}{\Delta t} \eta_k^n + AB\,\{G_k\}^n, \tag{20}$$

$$(\mathrm{D}^2 - \boldsymbol{k}^2)\xi_k^{n+1} - \eta_k^{n+1} = 0, \tag{21}$$

with $\mathrm{D} = \mathrm{d}/\mathrm{d}z$ and $AB\{f\}^n = (3f^n - f^{n-1})/2$ from the Adams–Bashforth formula. In the present form, the equations for η_k^{n+1} and ξ_k^{n+1} as well as those for ϕ_k^{n+1} and ζ_k^{n+1} are coupled. To solve these coupled equations we first eliminate ζ_k^{n+1} and η_k^{n+1}, which results in the two fourth-order equations

$$\left[\mathrm{D}^2 - \boldsymbol{k}^2 - R\,Ha \left(\frac{1}{\Delta t} + \frac{Ha}{R} \right) \right] [\mathrm{D}^2 - \boldsymbol{k}^2]\phi_k^{n+1} - \boldsymbol{k}^2 Ha^2 \phi_k^{n+1} = -\frac{R\,Ha}{\Delta t} \zeta_k^n + AB\{F_k\}^n, \tag{22}$$

$$\left[\mathrm{D}^2 - \boldsymbol{k}^2 - R\,Ha \left(\frac{1}{\Delta t} + \frac{Ha}{R} \right) \right] [\mathrm{D}^2 - \boldsymbol{k}^2]\xi_k^{n+1} - \boldsymbol{k}^2 Ha^2 \xi_k^{n+1} = -\frac{R\,Ha}{\Delta t} \eta_k^n + AB\{G_k\}^n. \tag{23}$$

The linear operator of fourth order on the left-hand side can be factorized into two operators of second order, namely

$$[\mathrm{D}^2 - \lambda_1][\mathrm{D}^2 - \lambda_2]\phi_k^{n+1} = -\frac{R\,Ha}{\Delta t} \zeta_k^n + AB\{F_k\}^n, \tag{24}$$

$$[\mathrm{D}^2 - \lambda_1][\mathrm{D}^2 - \lambda_2]\xi_k^{n+1} = -\frac{R\,Ha}{\Delta t} \eta_k^n + AB\{G_k\}^n. \tag{25}$$

In these equations, λ_1 and λ_2 are the real roots of the quadratic equation

$$\lambda^2 - \lambda \left[2\boldsymbol{k}^2 + R\,Ha \left(\frac{1}{\Delta t} + \frac{Ha}{R} \right) \right] + \boldsymbol{k}^4 + \boldsymbol{k}^2 \frac{R\,Ha}{\Delta t} = 0. \tag{26}$$

The factorization into second-order problems is convenient because the discretization of a one-dimensional Helmholtz equation with Chebyshev polynomials reduces to a tridiagonal system of linear algebraic equations, which can be solved very efficiently. It

is, however, not directly possible to satisfy the boundary conditions by the factorization approach, so that a Greens function technique becomes necessary. We shall explain this for the equation for ϕ_k^{n+1}; the problem for ξ_k^{n+1} is completely analogous. To obtain ϕ_k^{n+1}, we need to solve the system

$$[\mathrm{D}^2 - \lambda_1] f = -\frac{RHa}{\Delta t}\zeta_k^n + AB\{F_k\}^n, \tag{27}$$

$$[D^2 - \lambda_2]\phi = f, \tag{28}$$

where f denotes an auxiliary function, and the indices k and $n+1$ on ϕ are temporarily suppressed for notational convenience. Since there are no boundary conditions given for f, we need to find a general solution of the form

$$f = f^{(0)} + \lambda f^{(1)} + \mu f^{(2)}, \tag{29}$$

$$\phi = \phi^{(0)} + \lambda\phi^{(1)} + \mu\phi^{(2)}, \tag{30}$$

where $f^{(0)}$ satisfies the inhomogeneous equation (27) with zero boundary conditions, and $f^{(1)}$ and $f^{(2)}$ are the linearly independent solutions of (27) with zero right-hand side but non-zero boundary values, which we take as

$$f^{(1)}(1) = f^{(1)}(0) = 1, \tag{31}$$

$$f^{(2)}(1) = -f^{(2)}(0) = 1. \tag{32}$$

The functions $\phi^{(0)}$, $\phi^{(1)}$ and $\phi^{(2)}$ are solutions of (28) with right-hand side corresponding to $f^{(0)}$, $f^{(1)}$, $f^{(2)}$ and the known boundary conditions $\partial\phi/\partial z = 0$ at $z = 0, 1$. The unknown coefficients λ and μ are determined by applying the boundary conditions for ζ, which can be computed from ϕ. Since the timestep Δt in the numerical simulations is fixed, the auxillary functions $\phi^{(1)}$, $\phi^{(2)}$ and $f^{(1)}$, $f^{(2)}$ only have to be computed once at the start for each wave vector $\boldsymbol{k}$. They are stored and reused at every time step.

For the mean flow components U and V, time differencing gives

$$\left(\mathrm{D}^2 - \frac{R\,Ha}{\Delta t} - Ha^2\right) U^{n+1} = -\frac{R\,Ha}{\Delta t}U_k^n + R\,Ha\,AB\left\{\frac{\partial\langle v_x v_z\rangle}{\partial z} + \left\langle\frac{\partial p}{\partial x}\right\rangle + \frac{Ha}{R}\left\langle\frac{\partial\phi}{\partial y}\right\rangle\right\}^n, \tag{33}$$

$$\left(\mathrm{D}^2 - \frac{R\,Ha}{\Delta t} - Ha^2\right) V^{n+1} = -\frac{R\,Ha}{\Delta t}V_k^n + R\,Ha\,AB\left\{\frac{\partial\langle v_y v_z\rangle}{\partial z} + \left\langle\frac{\partial p}{\partial y}\right\rangle - \frac{Ha}{R}\left\langle\frac{\partial\phi}{\partial x}\right\rangle\right\}^n. \tag{34}$$

Together with the boundary conditions $U = V = 0$ at $z = 0$ and $z = 1$, these equations are again two one-dimensional Helmholtz problems. One can either prescribe the pressure gradient or volume fluxes, which are defined by

$$Q_x = \int_0^1 U(z)\,\mathrm{d}z, \quad Q_y = \int_0^1 V(z)\,\mathrm{d}z. \tag{35}$$

In the same way, either the mean potential gradients or the mean electric currents must be prescribed.

The flow solver that implements the numerical method has been developed to utilize the Message Passing Interface (MPI) for an efficient parallelization, since, even

at low resolutions, three-dimensional simulations demand a considerable amount of computational time. The algorithm is parallelized by assigning slices of the wave vector array to the individual processors (MPI threads). The array is sliced in the x-direction so that the wave vectors assigned to an individual processor cover some x-wavenumber range and the entire range of y-wavenumbers. Due to this approach, only the Fourier transformations require inter-process communication. The transpose method (Jackson, She & Orszag 1991) has been implemented to compute them. The program can be executed on a number of processors which is a power of 2 and which is smaller than the number of collocation points in the x- and y-directions.

For more information about the flow solver and the details relevant to the numerical method, time-integration scheme as well as parallelization technique refer to Boeck (2000).

2.3. *Procedure and parameters*

The transition to turbulence is complicated in itself and is also known to happen through several possible routes. One of these possibilities, as we mentioned before, is the so-called two-step scenario that implies, at the first stage, the existence of a disturbance in the form of two-dimensional streamwise vortices. The initial state of these two-dimensional vortices is specified by the spanwise and the vertical velocity components to form a pair of counter-rotating streamwise rolls in each near-wall shear region. The streamwise component of the velocity perturbation is initially zero. The streamwise vortices experience transient growth and evolve into streamwise streaks, whose most important property is the presence of inflection points in the velocity profile. If the streaks are sufficiently strong, the modulated flow may become unstable to random three-dimensional perturbations. The entire mechanism is referred to as *streak breakdown* (Schmid & Henningson 2001).

To verify the streak breakdown scenario in the case of MHD channel flow we split the numerical experiments into two steps to be carried out separately: two-dimensional and full three-dimensional simulations. A similar approach was employed in earlier stability investigations of other shear flows such as, for example, pipe flow (Zikanov 1996) or channel flow (Reddy *et al.* 1998).

First we solve the purely two-dimensional problem to investigate the optimal disturbances that initially take the form of streamwise vortices. We examine their evolution into streaks and dependence of the amplification of the perturbation energy on the flow parameters and the perturbation wavelength. We also compare the results of DNS with the linear predictions of Gerard–Varet (2002) to reveal the influence of the nonlinearity. In order to trace the streamwise vortices as purely two-dimensional structures the flow solver is modified, so that the fully nonlinear equations are solved with the flow dependence on the streamwise coordinate artificially suppressed. This is achieved by setting to zero the coefficients of the streamwise Fourier expansion, thereby switching off all the Fourier modes in the axial-direction besides the mean flow.

The second phase, with full three-dimensionality engaged, is the transition itself, i.e. the instability and breakdown of the streaks. The following procedure is utilized to investigate the mechanism of transition in accordance with the two-step scenario. As in the case of the purely two-dimensional problem, we specify the initial energy of the two-dimensional streamwise vortices and calculate the two-dimensional evolution until the energy of vortices grows to a certain level of amplification. At this time, three-dimensional random noise with given amplitude is imposed, while the artificial setting to zero of Fourier coefficients is switched off and simulation is continued as fully three-dimensional.

The details of flow parameters and periodicity lengths we have chosen for the runs, as well as the amplitudes of two-dimensional and three-dimensional perturbations, are outlined in the appropriate sections.

2.4. *Computational resolution*

The algorithm of fast Fourier transformation we used for the flow solver utilizes 2 as a basis-factor to compute the Fourier series. The resolution of a computational domain was restricted therefore to the numbers of collocation points in all directions being the power of 2, so that we used two different resolutions – 64^3 or 128^3 collocations points depending on the flow regime.

The numerical code was also verified by measuring the frequency αc_r and growth rate αc_i for an Orr–Sommerfeld mode from velocity time series of numerical simulations. The eigenvalues of the Orr–Sommerfeld problem were computed using a second-order finite-difference method, and the results were extrapolated to zero mesh size. This way, we obtained $\alpha c_r = 0.4738$ and $\alpha c_i = 0.0054$ for the fastest growing mode for $Ha = 1$, $Re = 20\,000$ and wavenumber $\alpha = 2$ (based on the channel width as lengthscale and the centreline velocity as velocity scale, and the timescale derived from these scales). The measured values from a simulation with 128 Chebyshev modes and $\Delta t = 2 \times 10^{-7}$ are $\alpha c_r = 0.47383$ and $\alpha c_i = 0.00535$.

To make sure that the flow solver can accurately represent fully developed turbulent flows, we performed a series of validation runs without the magnetic field. For the validation the results of the existing numerical study of turbulent channel flow by Kim, Moin & Moser (1987) were used. One of the reasons for choosing this study was that it used the pseudo-spectral approximation as well. We specified the same flow conditions, aspect ratio of the computational domain and the closest possible resolution (namely $128 \times 129 \times 128$). As we used the full channel width as a unit, our Reynolds number of 6600 corresponded to $Re = 3300$ based on the centreline velocity and channel half-width in the simulations by Kim *et al.* Accordingly, the Reynolds number Re_τ based on the wall shear stress velocity u_τ was found to be 360, that again corresponded to the value $Re_\tau = 180$ defined in terms of the channel half-width. Throughout this validation we compared the properties for turbulent flow, in particular mean velocity profiles, kinetic energy spectra of fully developed turbulence as well as profiles of root-mean-square velocity fluctuations and the Reynolds shear stress, normalized by the wall shear velocity u_τ. The comparison showed an almost exact coincidence of the numerical results; the slight disagreement could be attributed to different factors in the fast Fourier transformations, so that we were not able to set the same number of collocation points in the horizontal directions.

Before proceeding with simulations of flows affected by a magnetic field, a series of preliminary runs was performed to determine the relevant resolution of the computational domain for a particular range of the Hartmann numbers. With the increase of *Ha*, the boundary layers become thin. Since the process of turbulence onset is known to begin within the Harmann layer rather than in the bulk flow, the increase in *Ha* demands a corresponding refinement of the computational grid. Throughout the preliminary runs it was shown that, for Hartmann numbers up to 40, the computational resolution with 128^3 collocations points ensures that the results are reliable. However, to save computational time, the grid resolution was shrunk to 64^3 collocation points for *Ha* less than 20. Similar conclusions on the refinement of the computational grid for MHD turbulence can be found in Lee & Choi (2001), in particular the discussion on the relevance of computational resolution for finite

differences compared to that used in the pseudo-spectral approximation by Kim *et al.* for the non-MHD case.

All simulations were carried out in a computational domain with periodicity lengths $L_x = \pi$ in the streamwise direction and $L_y = 2\pi/Ha$ in the spanwise direction; the latter choice is discussed below in § 3.2. Addressing the streamwise periodicity length L_x being comparable to the whole layer thickness, we note that a further increase of L_x up to 2π left the results identical with respect to the conditions of instability and the beginning of evolution into fully developed turbulence. The fixed value Δt of the time step was chosen to ensure that the CFL conditions for the numerical stability are fulfilled.

3. Numerical results

3.1. *Transient growth and decay of two-dimensional perturbations*

In this section we analyse the temporal evolution of two-dimensional perturbations which are independent of the streamwise coordinate. We monitor the transient growth and decay of their energy and the development of their spatial structure. Particular attention is paid to the formation of inflection points for they are known to be the nuclei of instability and transition to turbulence in shear flows.

To show the details of the streak development for different parameters of the flow and to determine the effect of overlapping Hartmann layers (a possible source of the difference in stability characteristics between the channel and classical Hartmann flow), the simulations were performed for several combinations of R and Ha. The results of systematic computations of modulated two-dimensional flow at $R = 200$, 1000 and $Ha = 5$, 20 are presented in figures 2–5. In terms of the conventional Reynolds number, the four cases correspond to $(Re,\ Ha) = (1000, 5), (4000, 20), (5000, 5), (20\,000, 20)$. For each combination, we perform a series of simulations with the initial energy of two-dimensional perturbations varying between 10^{-5} and 10^{-1} of the energy of unperturbed channel flow; the energy is specified as follows:

$$E(t) = \frac{\iiint \boldsymbol{v}^2_{perturbatoin}\, \mathrm{d}^3\boldsymbol{r}}{\iiint \boldsymbol{v}^2_{basic\ flow}\, \mathrm{d}^3\boldsymbol{r}}.$$

All solutions in figures 2–5 share the common property that their kinetic energy grows, followed by a (not necessarily monotonic) decay. Additionally, for two of the selected regimes $(Re,\ Ha) = (4000, 20)$ and $(20\,000, 20)$, figure 6(a, b) gives insight into the spatial distribution of velocity profiles when the energy of two-dimensional perturbations achieves its maximum.

The typical evolution of the two-dimensional perturbations is presented in figure 7(a, b). The projection of the velocity field on a channel cross-section is shown for two different times. Initially, the two-dimensional perturbation is chosen in the form of streamwise rolls with zero streamwise velocity component V_x (figure 7, left). The subsequent evolution of two-dimensional perturbations is determined by the interaction between the rolls and the basic flow. The most important feature of the interaction is the transport of the streamwise velocity by vortical motions that results in growing distortion of the velocity profile. As a result, the streamwise velocity profile becomes a function of both y and z, which is also clearly seen in figure 6(a, b). One can see in figure 7 (right) that the amplitude of rolls decays with time. On the contrary, the amplitude of perturbations of the streamwise velocity component grows as illustrated in figures 2–5 by strong distortions of the mean velocity profile.

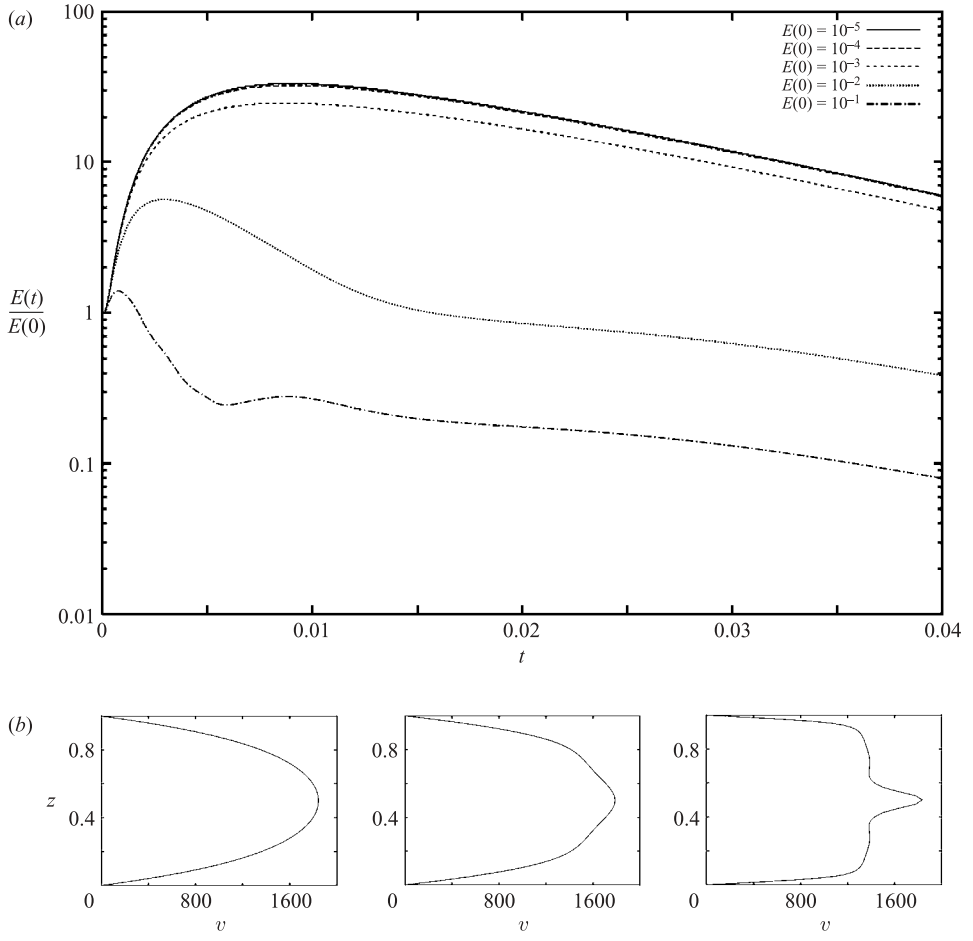

FIGURE 2. (*a*) Temporal evolution of the energy of two-dimensional perturbations for different values of the initial energy $E(0) = 10^{-5}$–10^{-1} and for $Re = 1000$, $Ha = 5$ ($R = 200$). (*b*) Spanwise-averaged velocity profiles of the modulated flow at the time when the energy of streamwise streaks has attained its maximum, for $Re = 1000$, $Ha = 5$, and three values of the initial energy $E(0)$ (from left to right): 10^{-5}, 10^{-3}, 10^{-1}.

Depending on the initial energy, *Re* and *Ha*, the evolution of two-dimensional perturbations may or may not involve a significant amplification of their total energy. Equally, the evolution may or may not lead to strong deformation of the velocity profile, formation of clearly visible streaks and occurrence of inflection points. Notice, however, that the concept of inflection points should be used with some caution because figures 2–5 show spanwise-averaged velocity profiles. Nevertheless, the presence of these features, as demonstrated in figure 6(*a*, *b*) with full velocity information, indicates a much stronger susceptibility to three-dimensional perturbations than in the unperturbed Hartmann profile.

The energy amplification depends strongly on the initial energy of two-dimensional perturbations, being a maximum for the infinitesimal perturbations with $E(0) = 10^{-5}$ and negligibly small for large-amplitude perturbations with $E(0) = 10^{-2}$ and $E(0) = 10^{-1}$. Another factor affecting the amplification is the Reynolds number (or parameter *R*). One can see in figures 2 and 4, and figures 3 and 5, that the flow with larger *Re* is,

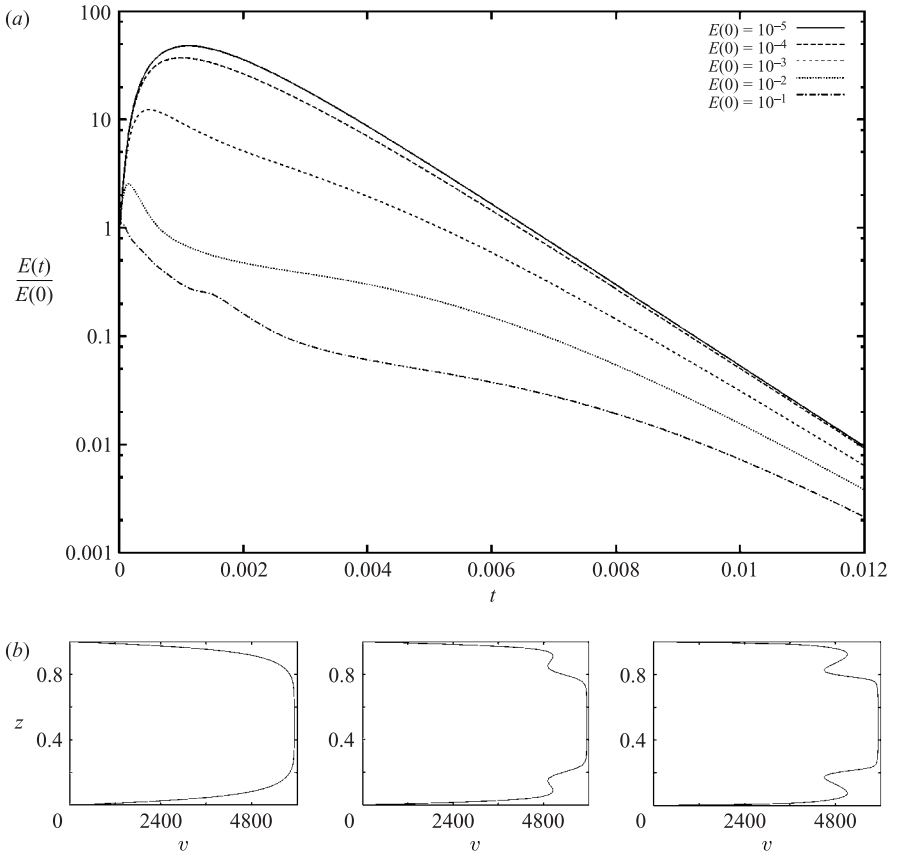

FIGURE 3. As figure 2 but for $Re = 4000$, $Ha = 20$ ($R = 200$).

indeed, more receptive to the instability since these cases experience stronger growth of two-dimensional streaks. To complete the discussion we would like to emphasize that it is not the amplification itself, but the maximum perturbation amplitude that is decisive for the flow transformation. Even after orders-of-magnitude growth, the perturbations with $E(0) = 10^{-5}$ are too weak to provide a significant modulation of velocity profile. On the contrary, the initially strong perturbations with $E(0) = 10^{-2}$ or $E(0) = 10^{-1}$, which experience almost no amplitude growth at all, are still strong enough to dramatically change the profile (figures 2*b*–5*b*, rightmost profiles).

The effect of the Hartmann number on the evolution of streamwise streaks becomes clearly recognizable when we compare the curves in figures 2 and 3 and figures 4 and 5. At equal R, changing Ha does not lead to any significant alteration of the amplification factor. It does, however, affect the typical timescale of the flow evolution. At higher Ha, both the initial growth and the subsequent decay of $E(t)$ occur at significantly higher rate. This certainly has a consequence for the flow stability characteristics. Any two-dimensional perturbation will eventually decay but, at smaller Ha, the three-dimensional instability of a two-dimensional modulated flow will have more time to develop. The effect of Ha on the development and decay of streaks can be explained by the stronger shear in the Harmann boundary layer corresponding to higher Ha. This provides more energy for the streak formation through interaction with the rolls but also facilitates faster streak dissipation.

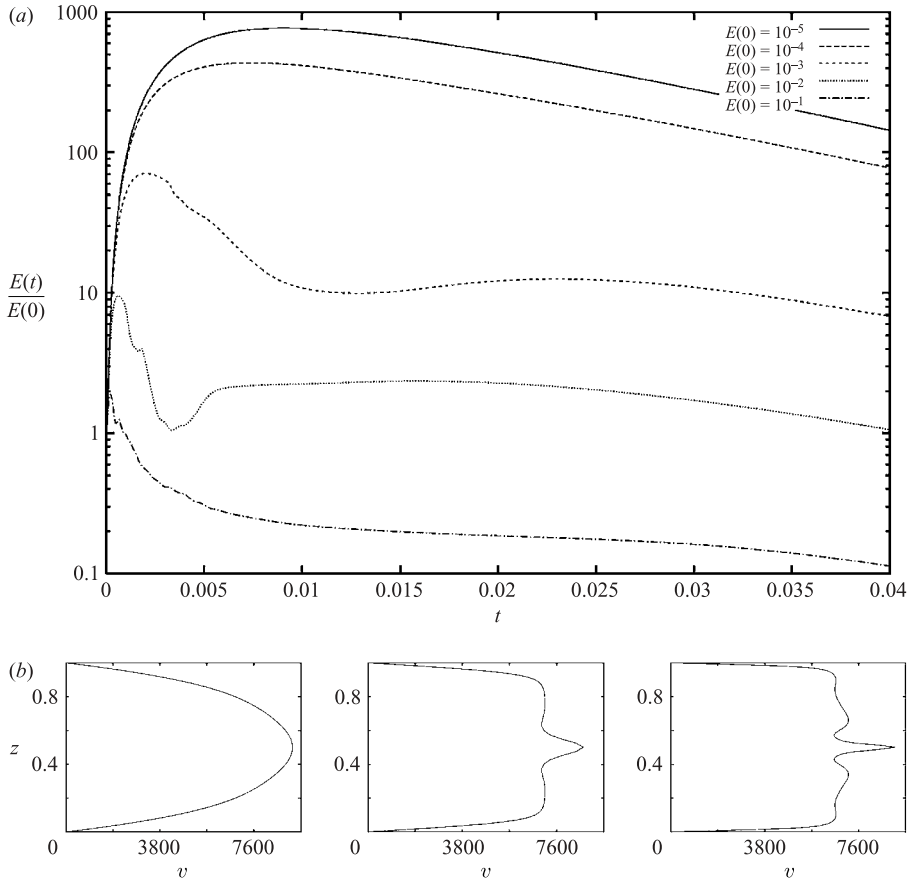

FIGURE 4. As figure 2 but for $Re = 5000$, $Ha = 5$ ($R = 1000$).

Our simulations allow us to see the effect of nonlinearity on the development of streaks. We cannot directly compare our results with the linear analysis of Gerard-Varet (2002), who found, for a single Hartmann layer, an amplification factor of 565.4 at $R = 1000$. We can however assume that our solutions for $E(0) = 10^{-5}$ follow closely the solution of a linearized problem. The assumption is supported by the fact that the curves for $E(0) = 10^{-5}$ and 10^{-4} nearly coincide in figure 2 and are very close in figure 3. Furthermore, the amplification factor of the 10^{-5} curves in figures 4 and 5 (both for $R = 1000$) has the order of 600, which is quite close to the linear analysis. The slight disagreement can be explained by different shape of initial streamwise vortices. One can see that, as the amplitude of two-dimensional perturbations grows, the nonlinear effects play an increasingly important role and the linear or weakly nonlinear theory similar to that of Gerard-Varet (2002) becomes increasingly misleading.

A comment should be made on the shape of the modulated velocity profiles. It can be seen in figures 2–6 that the shape is likely to be more and more complex with growing Re and $E(0)$. In particular, as many as eight inflection points might be counted in the profile at $Re = 5000$, $Ha = 5$, and $E(0) = 10^{-1}$; besides that, the effect of higher Re is clearly exposed in figures 6(a) and 6(b), which again highlights the potential for three-dimensional instability.

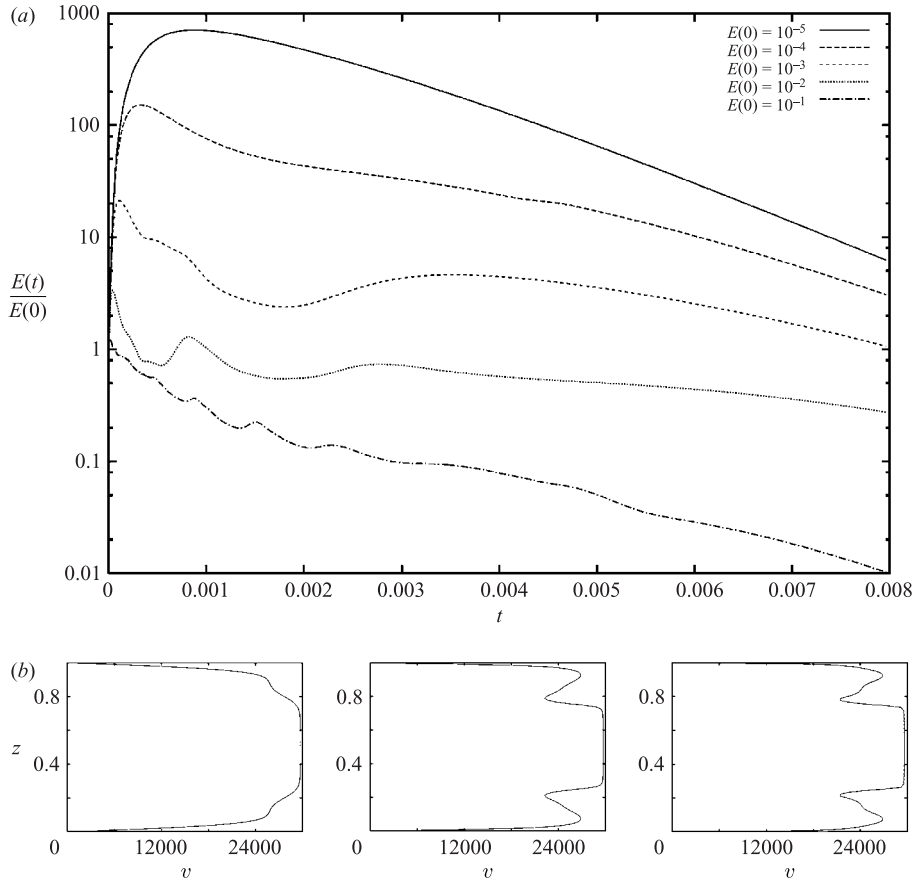

FIGURE 5. As figure 2 but for $Re = 20\,000$, $Ha = 10$ ($R = 1000$).

3.2. *Optimal spanwise length*

According to the linear analysis of two-dimensional perturbations of a Hartmann layer by Gerard-Varet (2002) the optimal perturbation that delivers the strongest growth of the initial energy has the form of streamwise-independent vortices (rolls) with a spanwise wavelength around $2\pi\delta$, where δ is the Hartmann layer thickness (more precisely, the value is slightly different in flows with electrically insulating and perfectly conducting walls). In our non-dimensional units, this *linearly optimal* wavelength corresponds to $L_y = 2\pi/Ha$. This value was used as the spanwise periodicity length (equal to the size of the computational domain) and as the spanwise wavelength of initial perturbations in the computations presented in § 3.1. Since, however, we saw above that the linear theory can be misleading, it is pertinent to verify whether the streamwise vortices with $L_y = 2\pi/Ha$ are indeed capable of providing the maximum growth for the nonlinear problem.

We performed additional computations of two-dimensional modulated flow for the two cases with $R = 200$, corresponding to $(Re, Ha) = (1000, 5), (4000, 20)$, with the spanwise periodicity length varying in the range π/Ha to $4\pi/Ha$. Two values of the initial energy of perturbations were used, namely $E(0) = 10^{-5}$ as a weak disturbance and $E(0) = 10^{-3}$ as a moderate one. The results are presented in figure 8 as the temporal evolution of the perturbation energy and in figure 9 as the amplification

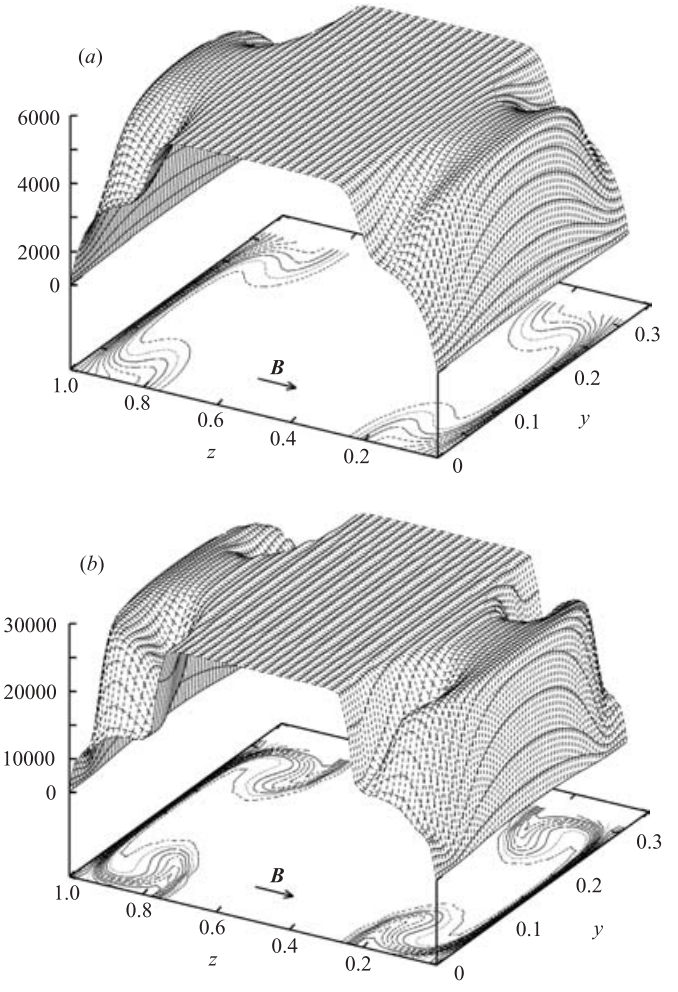

FIGURE 6. Spatial profiles and isolevels of the streamwise velocity component of the modulated flow at the time when the energy of streamwise streaks has attained its maximum. (*a*) $Re = 4000$, $Ha = 20$ ($R = 200$); (*b*) $Re = 20\,000$, $Ha = 20$ ($R = 1000$); the initial energy $E(0)$ is 10^{-3} for both cases (see figures 3 and 5).

factor versus the spanwise length. For our further discussion we find it convenient to introduce the abbreviation t_{opt} for the time when the kinetic energy of two-dimensional streamwise rolls has attained its maximum value, which we denote by E_{opt}.

One can see that two-dimensional perturbations are indeed affected by the spanwise wavenumber and they expose remarkable difference in the temporal behaviour. At the same time, the effect on the maximal kinetic energy the two-dimensional perturbations attain is not very significant. At small Ha, the perturbations with $L_y = \pi/Ha$ and $2\pi/Ha$ grow stronger than those with $L_y = 3\pi/Ha$ and $4\pi/Ha$. In the case of large Ha, which is more relevant to the Hartmann layer analysis of Gerard-Varet (2002), stronger growth is exhibited by the perturbations with $L_y = 2\pi/Ha$ and $3\pi/Ha$. The linearly optimal perturbations do not always experience the strongest growth. They, however, are invariably among the perturbations with the strongest growth, their amplification factor being less than 8% below the maximum. We conclude therefore, that, in terms of providing the maximum of amplification, the linear analysis points

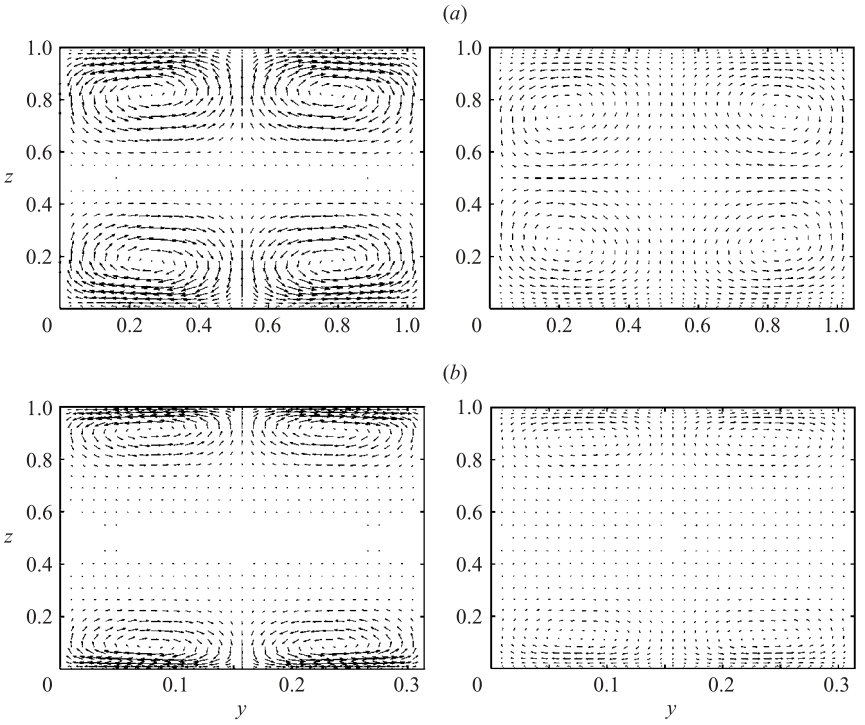

FIGURE 7. Evolution of two-dimensional perturbations at (*a*) $Re = 6000$, $Ha = 6$ ($R = 1000$); (*b*) $Re = 4000$, $Ha = 20$ ($R = 200$); y- and z-components of the velocity field are shown for the initial streamwise rolls (left) and for the moment when the energy of the perturbation has attained the maximum (right).

out the correct direction in which to search for optimal values of the spanwise periodicity length, and that the use of linearly optimal $L_y = 2\pi/Ha$ in our nonlinear computations is justified. Further, we shall use this value in all remaining simulations.

3.3. *Transition to turbulence and the full three-dimensional solution*

Our next step is to investigate the instability of the modulated flow followed by the transition using the features of the fully three-dimensional flow solver. Besides obtaining insight into the details of the two-step scenario that drives the instability mechanism, an attempt will be made to estimate the realistic critical R_c value for the transition to turbulence. To meet these goals the simulations are carried out following the algorithm outlined in § 3.1, applying two-dimensional perturbations first, then imposing three-dimensional noise to trigger the transition.

An example of the flow evolution with loss of stability followed by the transition to turbulence is presented on figure 10(*a*, *b*). The three-dimensional flow evolution shown by the solid curve in figure 10(*a*) corresponds to $Re = 6000$, $Ha = 6$, and the initial energy $E(0)$ of two-dimensional perturbations equal to 5×10^{-5}. The transient process is initiated by three-dimensional random noise with the amplitude $E_{3D} = 1.5 \times 10^{-14}$, imposed at the time $t_{opt} = 6 \times 10^{-3}$ of the maximum growth of perturbation energy. The dashed curve shows the flow evolution for the pure two-dimensional case. It can be seen in figure 10(*b*) that the three-dimensional perturbations of the modulated flow begin to grow a certain time after they are imposed and lead to streak breakdown (see the Appendix) and transition to turbulence at $t \approx 0.018$. We also present the

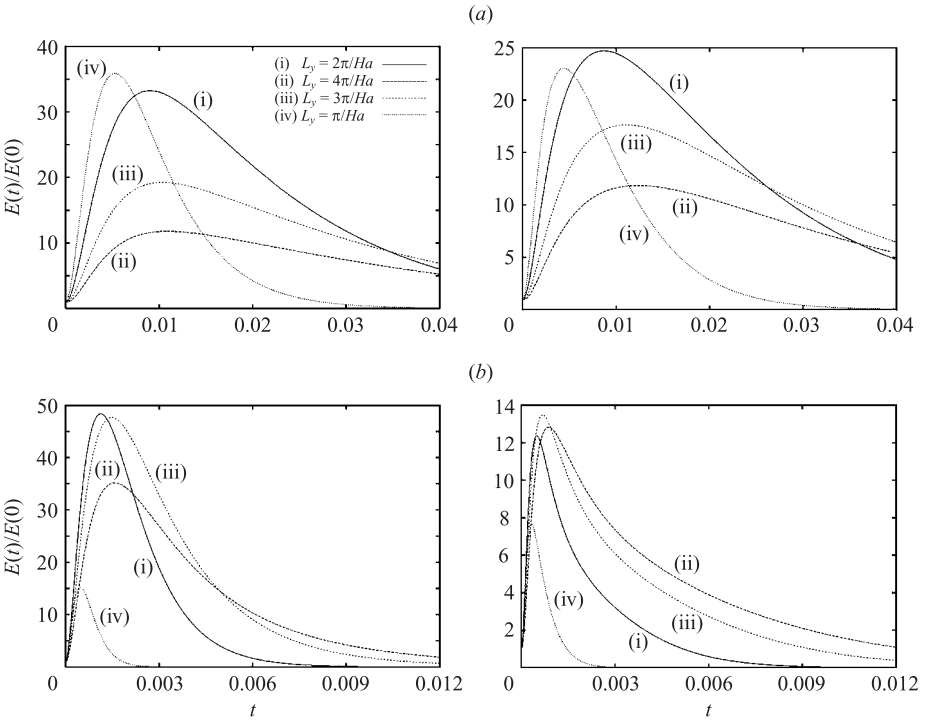

FIGURE 8. Temporal evolution of the energy of two-dimensional perturbations at different spanwise periodicity length. The solid curve corresponds to the 'optimal' periodicity according to the linear analysis. The parameters are (*a*) $Re = 1000$, $Ha = 5$ and (*b*) $Re = 4000$, $Ha = 20$, the initial energy of perturbations $E(0)$ is 10^{-5} (left) and 10^{-3} (right). $R = 200$ in all cases.

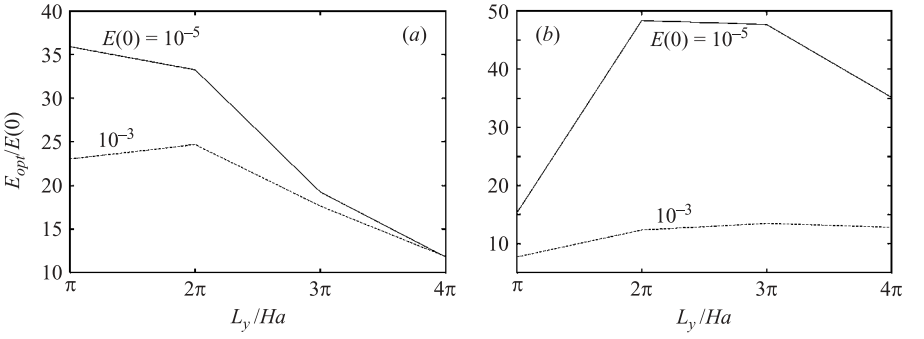

FIGURE 9. Ratio between the maximum energy of streamwise rolls (E_{opt}) and their initial energy as a function of spanwise length. (*a*) $Re = 1000$, $Ha = 5$; (*b*) $Re = 4000$, $Ha = 20$. $R = 200$ in all cases.

streamwise-independent component E_{2D} of the full three-dimensional field (dotted curve in figure 10*a*) to indicate how the kinetic energy of two-dimensional modulation decays in the process of streak breakdown. To demonstrate how soon the energy of pure three-dimensional perturbations begins to grow, the solid curve in figure 10(*b*) represents the difference between the full energy and the energy of the streamwise-independent component $E_{3D} - E_{2D}$ in the three-dimensional runs, whereas the dashed curve shows again the pure two-dimensional solution.

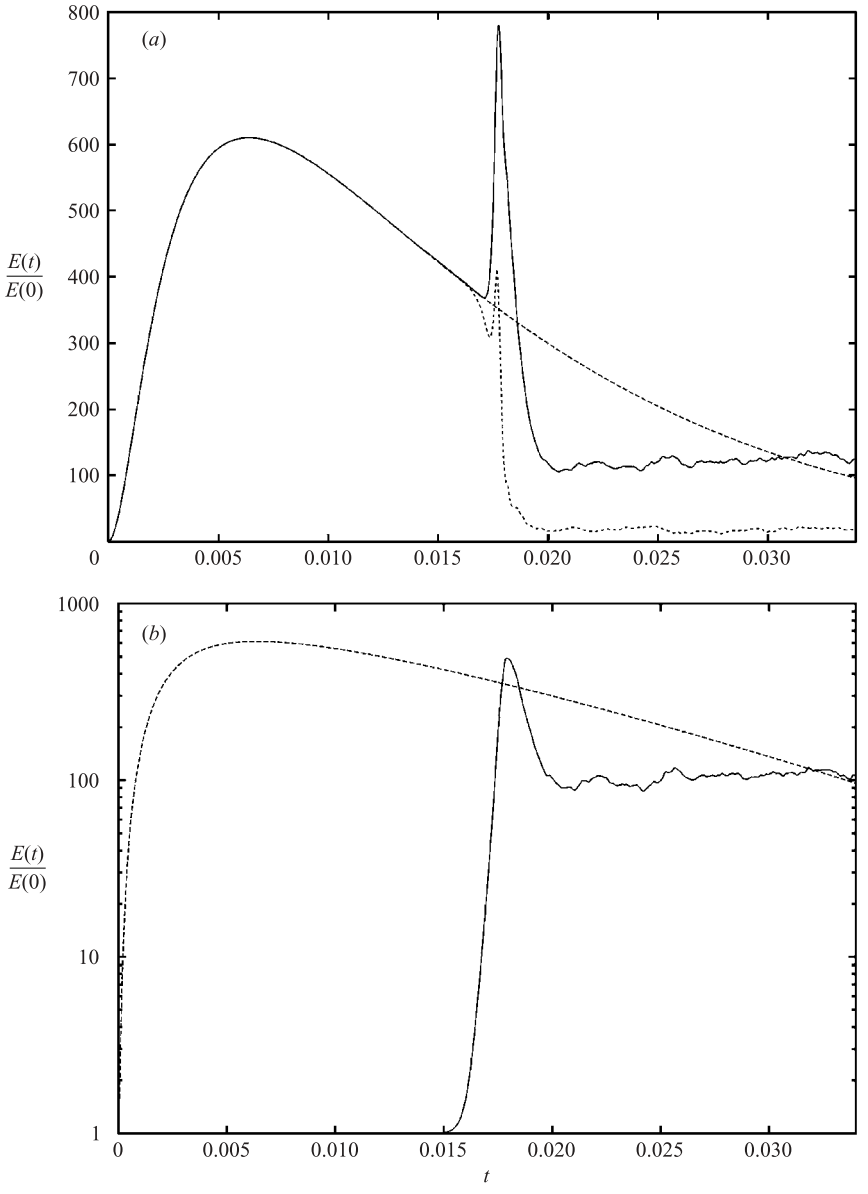

FIGURE 10. Transition to turbulence in MHD channel flow at $Re = 6000$, $Ha = 6(R = 1000)$. (*a*) Temporal evolution of the kinetic energy of two-dimensional optimal disturbances (– – – – –) and of fully three-dimensional flow (————) including the decay of two-dimensional modulation after the streak breakdown (- - - - - - -). (*b*) Growth rate of the kinetic energy of fully three-dimensional disturbances excluding the two-dimensional component (————) and the evolution in a pure two-dimensional run (– – – – –). The transition is obtained by adding three-dimensional random noise with amplitude 1.5×10^{-14} at $t_{opt} = 6 \times 10^{-3}$.

In real systems random infinitesimal three-dimensional perturbations always exist even for the case of a laminar flow. Hence, there is an opportunity for them to evolve and cause the flow instability before the two-dimensional streaks are fully developed, i.e. at $t < t_{opt}$. More precisely, we would like to know whether transition to turbulence can occur at a very early phase of the evolution, corresponding to $t < t_{opt}$. In order to

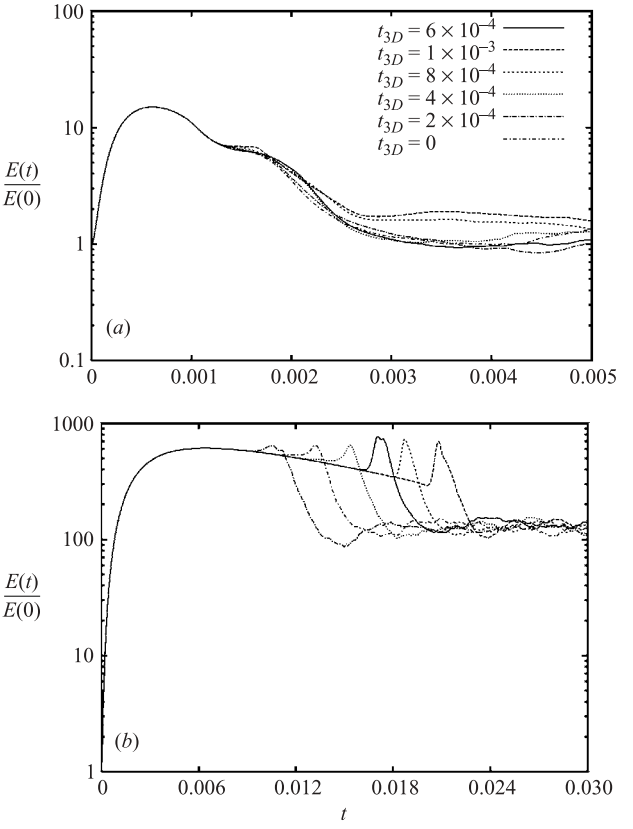

FIGURE 11. Transition to turbulence of the modulated flow at $Re = 6000$, $Ha = 6$ ($R = 1000$). Three-dimensional noise is imposed at different times t_{3D}, including the time of maximum growth of two-dimensional energy t_{opt} (solid curve). The initial energy of two-dimensional perturbations is (*a*) $E(0) = 5 \times 10^{-3}$ and (*b*) $E(0) = 5 \times 10^{-5}$.

clarify this issue we performed a series of simulations for $(Re, Ha) = (6000, 6)$, in which the moment t_{3D} when the three-dimensional random noise is imposed was varied. Two different values of the initial energy $E(0)$ of two-dimensional perturbations were used, namely 5×10^{-3} as a moderate disturbance and 5×10^{-5} as a weak one. A summary of these runs is presented through the time histories in figure 11, and as the moment t_{stall} of stability loss versus the moment t_{3D} of switching on three-dimensional random noise in figure 12. The abbreviation t_{stall}, that we introduce here, denotes the time when a strong growth of three-dimensional energy leads to a remarkable separation from the two-dimensional solution, manifesting the beginning of the transient process. In particular, we monitor the kinetic energy confined in the spanwise and the vertical velocity components, since this is found to make this separation clearly visible at the earliest stages of transition.

The results of these simulations clearly indicate that the above-mentioned premature transition never takes place. The transition always occurs at $t_{stall} > t_{opt}$ with the ratio t_{stall}/t_{opt} varying between 1.6 and 3.2. Assuming that the principal mechanism of instability is the energy transfer from two-dimensional modulated streaky flow to three-dimensional perturbations, this shows that only the fully developed streaks can provide sufficient energy input to trigger the transition. The effect is illustrated well in the

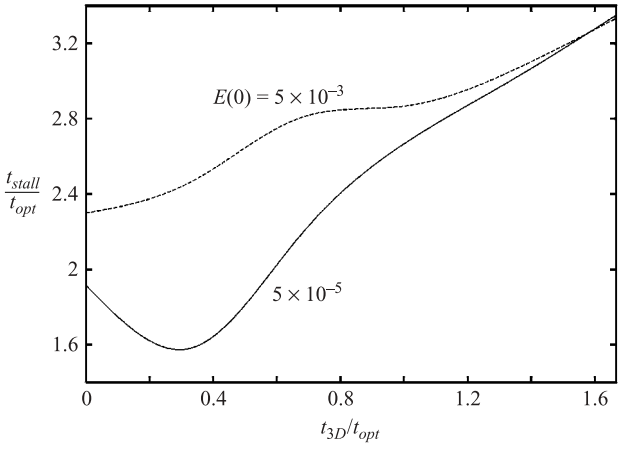

FIGURE 12. The beginning of instability (t_{stall}) vs. switching on three-dimensional noise (t_{3D}) for two values of the initial energy of streamwise vortices, $E(0) = 5 \times 10^{-5}$ and 5×10^{-3}; $Re = 6000$, $Ha = 6$ ($R = 1000$).

behaviour of the curve $E(0) = 5 \times 10^{-5}$ in figure 12. One can see that the transition occurs earlier for $t_{3D} = 2 \times 10^{-3}$ (local minimum on the solid curve) than for $t_{3D} = 0$. The explanation is that the energy of three-dimensional perturbations imposed at $t_{3D} = 0$ actually decays in the early stages of flow evolution when the streaks are underdeveloped.

Another illustration is found in figure 11(b): the perturbation energy is boosted to the highest level during the transition (the spike on the solid curve) when t_{3D} coincides with t_{opt}, i.e. when the two-dimensional energy has achieved its maximum. If the flow is modulated with stronger streamwise vortices, $E(0) = 5 \times 10^{-3}$, the process of the energy transfer from two-dimensional to three-dimensional perturbations proceeds much faster. Varying the time t_{3D} has a weaker effect on the time t_{stall} of the stability loss (figure 12, the dashed curve). One can assume that the dependence of t_{stall} on t_{3D} will be even weaker with further increase of the initial energy of the streamwise vortices. Also it is worthwhile to notice that the properties of the fully developed turbulent regime depend on Re and Ha only and are affected neither by t_{3D} nor by $E(0)$.

3.4. *Influence of the magnetic field on the turbulent flow and the process of streak breakdown*

It is well known that the properties of turbulent flows of electrically conducting liquids are strongly affected by the magnetic field. For the MHD channel and duct flows, numerous investigations (see Branover & Tsinober 1970) have revealed that there are two general ways in which the flow interacts with the transverse magnetic field. First is the Hartmann effect, the flattening of the mean flow profile. Secondly, not less important, is the transformation of turbulent vortices under the influence of a strong magnetic field. Theoretical (Davidson 1997) and numerical (Zikanov & Thess 1998) studies have revealed the most essential feature of the transformation: development of flow anisotropy associated with the elongation of vortices along the magnetic field lines. We cannot expect visible anisotropy to appear in our flow since the determining parameter of this process, the Stuart number $N = B_0^2 l\sigma/\rho_0 u$ is small: in our simulations its value is less than 1 (here l and u are typical length and velocity scales of a turbulent vortex). However, as demonstrated below, the magnetic field has a strong impact on the characteristics of turbulence and the process of streak breakdown.

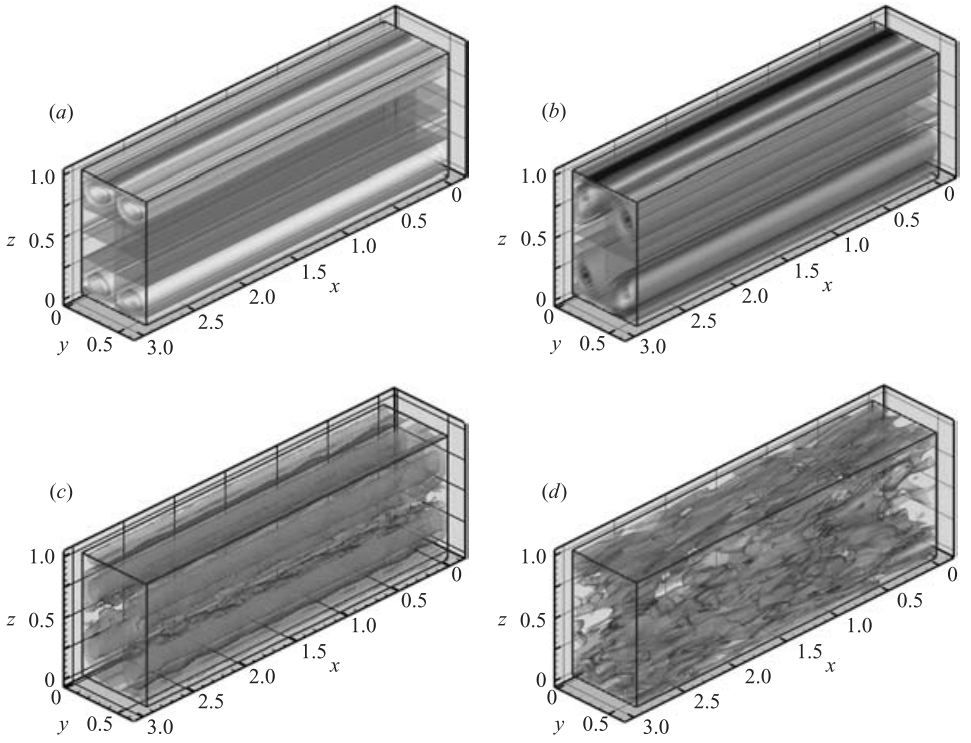

FIGURE 13. Isosurfaces of the streamwise vorticity component at $Re = 4000$, $Ha = 10$ ($R = 400$); four different phases of flow evolution: (*a*) initial state, (*b*) maximum growth of the energy of streamwise streaks t_{opt}, (*c*) streak breakdown $t \approx 4t_{opt}$ and (*d*) fully developed turbulence $t \gg t_{opt}$.

We carried out a series of numerical experiments for two flow regimes (Re, Ha) = (4000, 10) and (8000, 20). The combination of the parameters gives $R = 400$ for both cases, providing the same conditions in terms of stability, whereas the relatively high Ha allows these cases to be referred to as Hartmann flows rather than channel ones. Figures 13 and 14 show images taken from video sequences taken during these simulations. Four typical stages of the flow evolution resulting in the two-step scenario are presented by isosurfaces of the streamwise vorticity component: the initial state (*a*), the state of the maximum growth of the energy of streamwise streaks (*b*), the streak breakdown phase (*c*) and fully developed turbulence (*d*). For both runs the initial energy $E(0)$ of the two-dimensional streamwise vortices and the amplitude of three-dimensional noise, imposed at time t_{opt}, is 10^{-3} and 3×10^{-6}, respectively.

The most remarkable difference between the two regimes can be observed in figures 13(*d*) and 14(*d*) that show fully developed turbulent states. One can see that for the case of $Re = 4000$ and $Ha = 10$ the bulk flow is involved in the process of turbulence generation, which begins as the streak breakdown occurs, and, as a result, vortical perturbations dilate over the whole cross-section of a computational domain. At stronger magnetic field, in the case with $Re = 8000$, $Ha = 20$, the turbulence generation happens in relatively thin regions near the walls, and, unlike the former case, the core flow remains almost undistorted (figure 14*d*). In the subsequent flow evolution, the turbulent eddies remain confined to the localized areas of strong shear flow near the walls. If we compare figures 13(*b*, *c*) and 14(*b*, *c*), the conclusion can

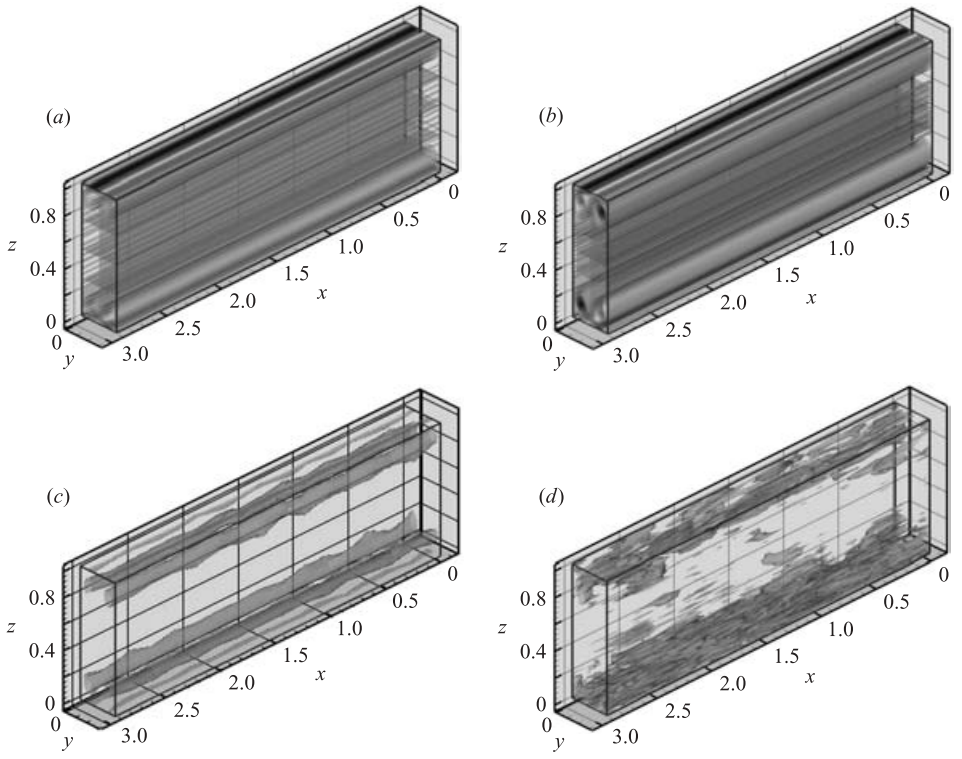

FIGURE 14. As figure 13 but at $Re = 8000$, $Ha = 20$ ($R = 400$).

be drawn that the difference between the turbulent regimes originates in the earlier stages of transition, i.e. the streak breakdown phase. Stronger magnetic field limits the streak breakdown to near-wall regions and prevents the turbulent fluctuations from spreading into the bulk flow.

3.5. *Critical R value*

Using the two-step scenario we are able to describe the process of transition to turbulence starting from the earliest stages. However, there is one important question, which has been left aside so far: does the proposed scenario provide a critical value of R for the transition to turbulence that is in agreement with the recent experimental result $R_c \approx 380$ of Moresco & Alboussière (2004). One has to realize, of course, that, contrary to the transition triggered by the linear instability mechanism, the transient scenario considered in this paper does not have a sharp stability threshold. Theoretically, the transition to turbulence can or cannot occur at any given value of R in the range between the limits of energetic and linear stability, depending on the amplitude and form of two-dimensional and three-dimensional perturbations.

We can, however, attempt to verify the validity of the proposed scenario through comparison of the experimental results with the simulations at realistic amplitudes of two-dimensional and three-dimensional noise. For this purpose, we carried out a series of runs for different flow regimes starting from $R = 200$ and increasing its value gradually. The Hartmann number was kept constant at $Ha = 10$. The initial energy $E(0)$ of the streamwise rolls and the initial amplitude $E_{3D}(t_{opt})$ of the random noise were varied up to 10^{-1} and 10^{-3} correspondingly.

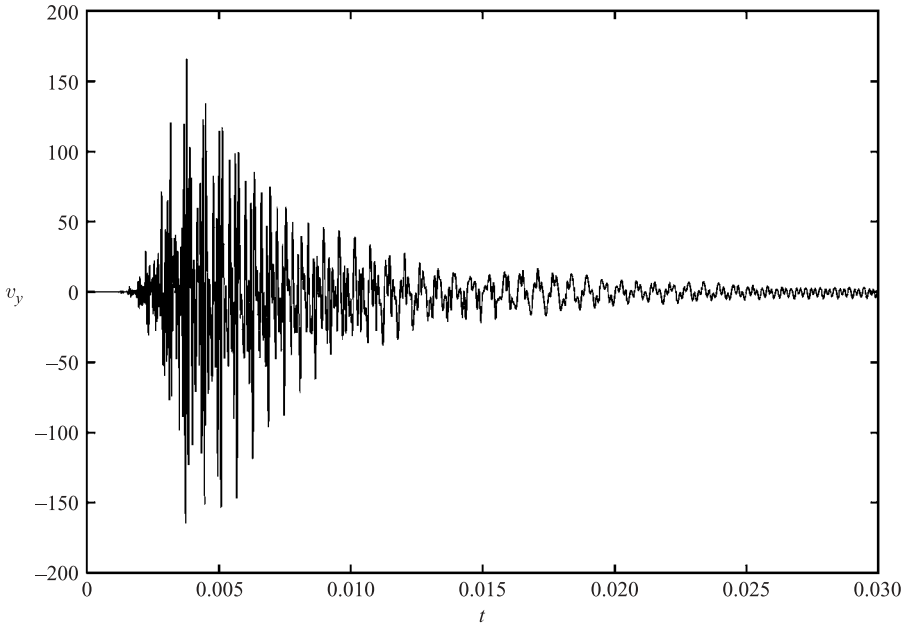

FIGURE 15. Temporal flow evolution at $R = 350$ ($Re = 3500$, $Ha = 10$) and subcritical two-dimensional modulation $E(0) = 8 \times 10^{-3}$. Oscillogram of the spanwise velocity component in the region of formation of the inflection points. The initial growth is eventually followed by re-laminarization.

No transition to turbulence was found at $R < 350$. All our attempts ended with re-laminarization of the flow for small-amplitude three-dimensional noise below 10^{-3} or numerical instability caused by the overcharged three-dimensional perturbations. At high values of R, approximately $R > 400$, the transition occurred every time the amplitude of two-dimensional perturbations was sufficient for the inflection points to develop. Some minimum amplitude of three-dimensional noise needed to be exceeded to trigger the instability. This amplitude, which could be easily determined in the calculations, varied with R and $E(0)$.

For the intermediate values $350 \leqslant R < 400$ a peculiar behaviour of modulated two-dimensional flow was observed. If the initial energy of the two-dimensional flow was below a certain level, no transition occurred regardless of the amplitude of three-dimensional perturbations imposed afterwards. A slight increase of $E(0)$ above this level made it possible to find the amplitude of three-dimensional noise that triggered the transition. It is important to remark that visual inspection of both 'stable' and 'unstable' two-dimensional modulated flow revealed similar streaks with well-developed inflection points so that the instability was not correlated directly with the presence of these features. In the other words, the inflection points themselves cannot be regarded as definite nuclei of potential flow instability for this range of R, but, instead, a certain level of two-dimensional energy has to be overcome for the modulated flow to perceive the three-dimensional noise.

The difference between the stable and unstable evolutions in the intermediate range of R is seen in figures 15 and 16, which show the signals of the spanwise velocity component in the region where the inflection points are formed. Both show the case with $(Re,\ Ha) = (3500, 10)$, $R = 350$, and the initial energy $E(0)$ of the two-dimensional modulation is 8×10^{-3} and 10^{-2} respectively, whereas the initial

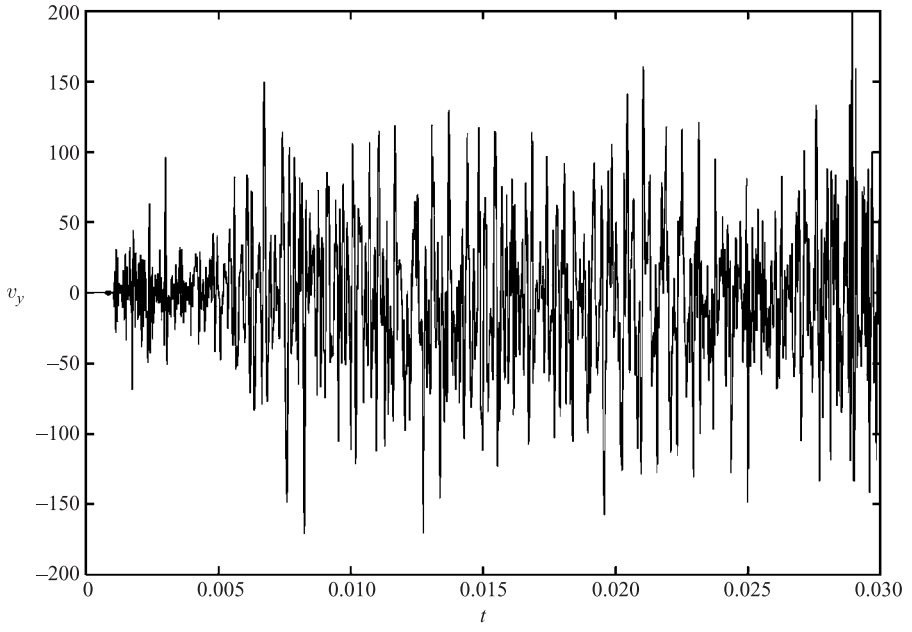

FIGURE 16. Temporal flow evolution at $R = 350$ ($Re = 3500$, $Ha = 10$) and supercritical two-dimensional modulation $E(0) = 10^{-2}$. Oscillogram of the spanwise velocity component in the region of formation of the inflection points. Three-dimensional instability of the modulated flow results in the transition to turbulence.

amplitude of the random noise is $E_{3D}(t_{opt}) = 10^{-4}$ for both cases. Despite the fact that the magnitude of the two-dimensional perturbations is strong enough to form inflection points in both cases, the evolution yields two separate possibilities, i.e. re-laminarization (figure 15) and transition to turbulence (figure 16). During the initial phase both flows experience a transient growth accompanied by oscillations, whose frequency is apparently a characteristic for a given set of parameters. The subsequent evolution is exhibited in a distinct way: one can see the decay of perturbations in figure 15 and the stochastic process in figure 16 with all timescales involved. The critical modulation, i.e. the initial amplitude of two-dimensional energy necessary to trigger the energy transfer from two-dimensional to three-dimensional perturbations, exists for any $R_{energy} < R < R_{linear}$. We can say that, for the flow with $Re = 3500$ and $Ha = 10$ ($R = 350$) we determined that the *critical modulation* lies between 8×10^{-3} and 10^{-2}.

We also performed a series of simulations for the flow regime with $Re = 7000$ and $Ha = 20$ (R is again kept equal to 350), to make sure that the phenomenon described above is controlled by R. The results of these runs reveal similar behaviour of the two-dimensional and three-dimensional perturbations. As in the case above, a slight variation of $E(0)$ around 10^{-2} produces either re-laminarization or flow instability.

4. Concluding remarks

The processes of loss of stability and transition to turbulence in the Hartmann flow were studied using the numerical solution of fully nonlinear Navier–Stokes equations.

A two-step mechanism, proposed as the transition scenario, was investigated to explain the genesis of instability and further evolution towards fully developed turbulence. According to this scenario, the unperturbed flow is modulated by two-dimensional optimal disturbances, which experience a large transient growth and modify the basic flow so that it becomes unstable to small three-dimensional random perturbations. The initial flow modulation providing an optimal perturbation (i.e. the one with the maximum growth of perturbation energy) was shown to have the form of two-dimensional streamwise rolls. The scenario was introduced for non-magnetic shear flows (see Grossmann 2000 and Schmid & Henningson 2001 for review) and extended in this paper to a specific case of MHD Hartmann flow.

The two-dimensional streamwise perturbations and the to comparison of their evolution with known results of the linear analysis (Gerard-Varet, 2002) were considered separately. The simulations have shown that if the two-dimensional perturbations are very weak, the entire flow evolution closely follows the linear analysis predictions. For any substantial initial energy of two-dimensional perturbations, the nonlinear effects proved important, so the linear approach was shown to be misleading. We studied the spatial structure of the streamwise vortices and found that the circumferential velocity component of the rolls decays rapidly, the rolls being transformed into streamwise streaks in full agreement with the theory. Our search for the optimal spanwise wavelength of the two-dimensional perturbations (the wavelength that provides strongest transient amplification) led to the conclusion that the results of the linear analysis of Gerard-Varet (2002) are applicable to the fully nonlinear case. The amplification factor was found to be only slightly sensitive to the wavelength in a wide range around $2\pi\delta$.

Our computations confirmed the role of inflection points in the two-dimensional modulated velocity profiles as the nuclei for three-dimensional instability. In the calculations with small R and weak initial two-dimensional perturbations, where inflection points did not appear, the flow remained stable to three-dimensional perturbations of any reasonable amplitude.

One of the goals of this work was to find a theoretical explanation of the recent experimental results of Moresco & Alboussière (2004), who found $R_c \approx 380$ as the critical parameter value, above which sustained turbulence can exist in a channel with smooth walls. This value is about two orders of magnitude lower than the stability limit predicted by the linear analysis.

According to the nature of the instability mechanism proposed in this paper, there can be no sharp stability threshold but, rather, a range of values of R in which the flow can be stable or unstable depending on the amplitude of perturbations. A confirmation of that can also be found in Moresco & Alboussière (2004). The stability of the experimental flow was very sensitive to the roughness of the walls, i.e. to the amplitude of random noise introduced into the flow. Our calculations showed that, at the perturbation amplitude typical for the smooth-wall experiments, the critical value R_c lies between 350 and 400, i.e. good agreement with Moresco & Alboussière (2004) was achieved. Furthermore, the computations stressed the importance of the critical amplitude of two-dimensional perturbations that has to be exceeded for the instability to occur.

A final remark should be made about the usefulness of simulations at moderate Hartmann numbers of the order $Ha \approx 10$. In the past, most MHD experiments have been carried out in (opaque) liquid metals with magnetic fields $B \approx 1$ T, resulting in Hartmann numbers of the order $Ha \approx 300$, which is much higher than in the numerics.

However, with the advent and broad availability of superconducting magnets, capable of producing magnetic fields of more than $B \approx 10\,\mathrm{T}$, experiments on Hartmann flows in transparent liquids will become possible in the foreseeable future. Such flows are characterized by Hartmann number as low as $Ha \approx 10$ but can be visualized and measured using non-contact flow measuring techniques. Thus our numerical predictions for moderate Ha will be amenable to direct experimental tests.

Summarizing the results of this work, we conclude that the proposed scenario is indeed one of the transition possibilities that provides a self-sufficient explanation of experimentally observed instability and transition to turbulence in the MHD channel flow.

The authors express their gratitude to the DFG for financial support in the frame of the "Research Group Magnetofluiddynamics" at the Ilmenau University of Technology. O. Zikanov was partially supported by the grant from the Rakham graduate school, University of Michigan. T. Boeck is supported by the DFG under the grant Bo 1668/2-1. The simulations were carried out on a CRAY T3E supercomputer, access to which was provided by the John von Neumann Institute (NIC) at the Forschungszentrum Jülich. The authors also thank Professor Yu. Kolesnikov, Dr O. Andreev and the referees for careful reading and useful comments.

Appendix

We performed an additional numerical experiment – the calculation of the transient process starting from small-amplitude random three-dimensional noise imposed on the basic flow. At certain stages of the evolution, elongated streamwise structures (streaks) were detected. The results of these runs are outlined here in figures 17 and 18; the parameters of the simulation, i.e. the Reynolds number, the resolution and the aspect ratio of the computational domain, were chosen to follow the numerical study of turbulent channel flow by Kim *et al.* (1987).

Figure 17(a, b) demonstrates the transient process at $Re = 6600$ and $Ha = 15$ started with initial perturbations specified as three-dimensional random noise of amplitude $E_{3D}(0) = 10^{-4}$ with respect to the energy of the unperturbed flow. Two curves in figure 17(a) show the temporal evolution of the full three-dimensional energy of perturbations E_{3D} (——————) and energy of the streamwise-independent flow modes $E(k_x = 0)$ (– – – – –) confined in the Fourier space as the modes with wavenumbers $k_x = 0$. In the case of the two-step scenario considered in the paper, this sub-range of the Fourier space contains the streamwise rolls which develop into streaks. Figure 17(b) shows the distribution of streamwise-independent energy $E(k_x = 0)$ over the velocity components. Observing the temporal evolution presented in the figures, one may conclude that two processes take place. First, the full energy of the perturbations converges to the streamwise-independent energy subset, for the latter has the longest lifetime (figure 17a). On the other hand, the streamwise-independent energy is redistributed so that, after a short time period, it is almost completely transferred to the streamwise velocity component (figure 17b). It can be shown that the transport of energy towards the streamwise velocity component, i.e. the development of streamwise elongated streaks, is a particular feature of shear flows caused by the nonlinear mechanism.

The formation of streaks is also illustrated in figure 18. The set of frames (a)–(f) shows the temporal evolution of an arbitrary three-dimensional random noise imposed

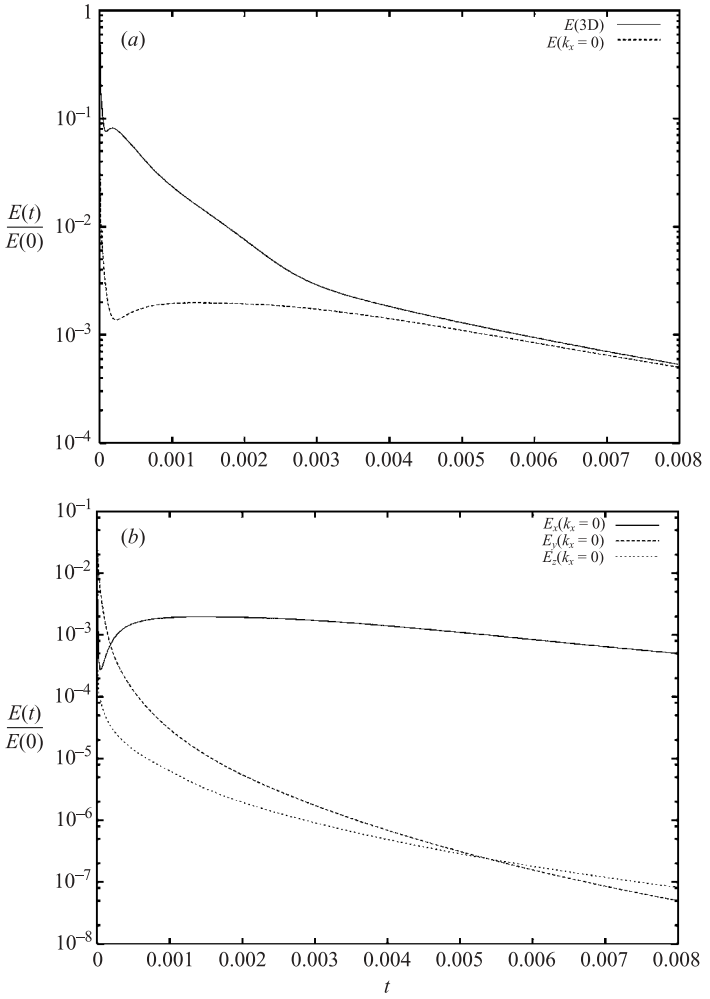

FIGURE 17. Transient process resulting form three-dimensional random noise: (*a*) temporal evolution of full three-dimensional energy of perturbations E_{3D} (————) and its component $E(k_x = 0)$ in the sub-range of the Fourier space with wavenumbers $k_x = 0$ (– – – – –); (*b*) transport of the energy $E(k_x = 0)$ in the streamwise direction, separate energies of streamwise (————), spanwise (– – – – –) and vertical (- - - - - - -) velocity components; $Re = 6600$, $Ha = 15$, $E_{3D}(0) = 10^{-4}$.

at the initial state. The isosurfaces of streamwise velocity fluctuations demonstrate that the flow transformation is accompanied by the appearance of structures elongated in the axial direction. Besides that, we have also performed simulations both for the non-magnetic case and for $Ha = 6$. However, the case of higher Hartmann number was chosen to highlight the point that the process of elongation into streak-like pattern becomes more efficient in the regions where the shear stresses are concentrated and, therefore, the mechanism of energy transport into the streamwise component is stronger. Summing up, the evolution of three-dimensional random perturbations is shown to result in the pattern with clearly recognizable streak-like structures elongated in the streamwise direction. Our choice of the streak breakdown mechanism is, therefore, by no means artificial.

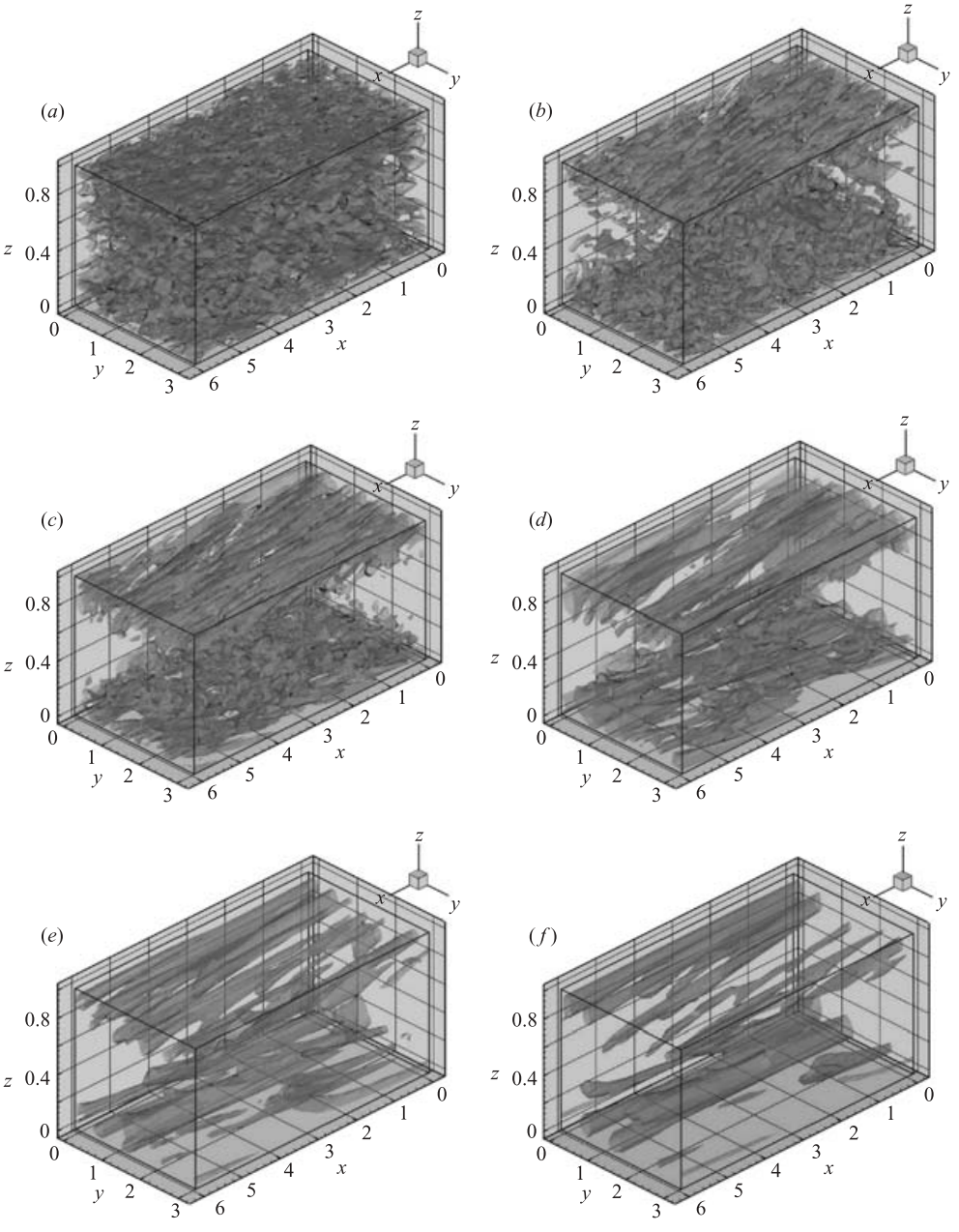

FIGURE 18. Temporal evolution of initially imposed three-dimensional random noise into the pattern with streak-like structures elongated over the streamwise direction: the isosurfaces of the streamwise velocity fluctuations at $Re = 6600$, $Ha = 15$, $E_{3D}(0) = 10^{-4}$.

REFERENCES

BOECK, T. 2000 *Bérnard-Marangoni Convection at low Prandtl Numbers. Results of Numerical Simulation.* Shaker Verlag, Aachen.

BOECK, T. & THESS, A. 1999 Bérnard–Marangoni convection at low Prandtl numbers. *J. Fluid Mech.* **399**, 251–275.

BRANOVER, G. 1967 Resistance of magnetohydrodynamic channels. *Magnetohydrodynamics* **3**, 1–11.

Branover, G. & Tsinober, A. 1970 *Magnetohydrodynamics of Incompressible Fluids*. Nauka, Fys. Mat. Lit., Moscow.

Canuto, C., Hussaini, M. Y., Quarteroni, A. & Zang, T. 1998 *Spectral Methods in Fluid Dynamics*. Springer.

Davidson, P. A. 1997 The role of angular momentum in the magnetic damping of turbulence. *J. Fluid Mech.* **336**, 123–150.

Davidson, P. A. 2000 An energy criterion for the linear stability of conservative flows. *J. Fluid Mech.* **402**, 329–348.

Davidson, P. A. 2001 *An Introduction to Magnetohydrodynamics*. Cambridge University Press.

Gerard-Varet, D. 2002 Amplification of small perturbations in a Hartmann layer. *Phys. Fluids* **14**, 1458–1467.

Gottlieb, D. & Orszag, S. A. 1977 Numerical analysis of spectral methods. *CBMS-NSF Reg. Conf. Series in Appl Maths, Philadelphia.*

Grossmann, S. 2000 The onset of shear flow instability. *Rev. Mod. Phys.* **72**, 603–618.

Hartmann, J. & Lazarus, F. 1937 Experimental investigations on the flow of mercury in a homogeneous magnetic field. *K. Dan. Vidensk. Selsk. Mat. Fys. Medd.* **15**(7), 1–45.

Jackson, E., She, Z.-S. & Orszag, S. A. 1991 A case study in parallel computing: I. Homogeneous turbulence on a hypercube. *J. Sci. Comput.* **6**, 27–45.

Kim, J., Moin, P. & Moser, R. 1987 Turbulence statistics in fully developed channel flow at low Reynolds number. *J. Fluid Mech.* **177**, 133–166.

Lee, D. & Choi, H. 2001 Magnetohydrodynamic turbulent flow in a channel at low magnetic Reynolds number. *J. Fluid Mech.* **429**, 367–394.

Lingwood, R. J. & Alboussière, T. 1999 On the stability of the Hartmann layer. *Phys. Fluids* **11**, 2058–2068.

Lock, R. C. 1955 The stability of the flow of an electrically conducting fluid between parallel planes under a transverse magnetic field. *Proc. R. Soc. Lond.* A **233**, 105–125.

Lundquist, S. 1952 Studies in magneto-hydrodynamics. *Ark. Fys.* **5**, 297.

Lykoudis, P. S. 1960 Transition from laminar to turbulent flow in magneto-fluid mechanic channels. *Rev. Mod. Phys.* **32**, 796–798.

Moresco, P. & Alboussière, T. 2004 Experimental study of the instability of the Hartmann layer. *J. Fluid Mech.* **504**, 167–181.

Murgatroyd, W. 1953 Experiments on magneto-hydrodynamic channel flow. *Phil. Mag.* **44**, 1348–1354.

Reddy, S. C., Schmid, P. J., Bagget, P. & Henningson, D. S. 1998 On stability of stream-wise streaks and transition thresholds in plane channel flow. *J. Fluid Mech.* **365**, 269–303.

Roberts, P. H. 1967 *An introduction to Magnetohydrodynamics*. Longmans.

Schmid, P. J. & Henningson, D. S. 2001 *Stability and Transition in Shear Flows*. Springer.

Takashima, M. 1996 The stability of the modified plane Poiseulle flow in the presence of a transverse magnetic field. *Fluid Dyn. Res.* **17**, 293–310.

Takashima, M. 1998 The stability of the modified Couette flow in the presence of a transverse magnetic field. *Fluid Dyn. Res.* **22**, 105–121.

Thual, O. 1992 Zero-Prandtl-number convection. *J. Fluid Mech.* **240**, 229–258.

Zikanov, O. 1996 On the instability of pipe Poiseuille flow. *Phys. Fluids* **8**, 2923–2932.

Zikanov, O. & Thess, A. 1998 Direct numerical simulation of forced MHD turbulence at low magnetic Reynolds number. *J. Fluid Mech.* **358**, 299–333.